2021-12

Working paper. Economics

ISSN 2340-5031

ROBUST ESTIMATION AND FORECASTING OF CLIMATE CHANGE USING SCORE-DRIVEN ICE-AGE MODELS

Szabolcs Blazsek and Álvaro Escribano

uc3m | Universidad Carlos III de Madrid

Serie disponible en http://hdl.handle.net/10016/11

Web: http://economia.uc3m.es/

Correo electrónico: departamento.economia@eco.uc3m.es

Robust Estimation and Forecasting of Climate Change Using Score-Driven Ice-Age Models

Szabolcs Blazsek [a] and Alvaro Escribano [b,*]

[a] School of Business, Universidad Francisco Marroquín, 01010, Guatemala, Guatemala; sblazsek@ufm.edu

[b] Department of Economics, Universidad Carlos III de Madrid, 28903, Madrid, Spain; alvaroe@eco.uc3m.es

Abstract: Score-driven models applied to finance and economics have attracted significant attention in the last decade. In this paper, we apply those models to climate data. We study the robustness of a recent climate econometric model, named ice-age model, and we extend that model by using score-driven filters in the measurement and transition equations. The climate variables considered are Antarctic ice volume Ice_t, atmospheric carbon dioxide level $\text{CO}_{2,t}$, and land surface temperature Temp_t, which during the history of the Earth were driven by exogenous variables. The influence of humanity on climate started approximately 10-15 thousand years ago, and it has significantly increased since then. We forecast the climate variables for the last 100 thousand years, by using data for the period of 798 thousand years ago to 101 thousand years ago for which humanity did not influence the Earth's climate. For the last 10-15 thousand years of the forecasting period, we find that: (i) the forecasts of Ice_t are above the observed Ice_t, (ii) the forecasts of the $\text{CO}_{2,t}$ level are below the observed $\text{CO}_{2,t}$, and (iii) the forecasts of Temp_t are below the observed Temp_t. Our results are robust, and they disentangle the effects of humanity and orbital variables.

Keywords: climate change; ice-ages and inter-glacial periods; atmospheric CO_2 and land surface temperature; dynamic conditional score models; generalized autoregressive score models

*Corresponding author. Postal address: Department of Economics, Universidad Carlos III de Madrid, Calle Madrid 126, Getafe (Madrid), 28903, Spain. E-mail: alvaroe@eco.uc3m.es, Phone: +34 91 624 9854

1. Introduction

Climate change is the most important global issue on the Earth. According to the Intergovernmental Panel on Climate Change (2021), compared to the period of 1850 to 1900, the Earth's global surface temperature for the period of 2081 to 2100 is very likely to rise by 1.0 to 1.8 Celsius degrees under the "very low greenhouse gas emissions scenario", by 2.1 to 3.5 Celsius degrees for the "intermediate scenario", and by 3.3 to 5.7 Celsius degrees under the "very high greenhouse gas emissions scenario". The worst-case scenario implies dramatic consequences on the nature and wildlife in terrestrial, wetland, and ocean ecosystems, and on humanity with respect to food and water security, migration, health, higher risk of conflict worldwide, reduction of global economic product, and a possible collapse of the current societal organization.

Humanity has existed for 6,000,000 years and the modern human form evolved around 300,000 years ago. Climate change is partly due to the influence of humanity on the Earth's climate, which started approximately 10-15 thousand years ago, by commencing agricultural activities such as cultivating plants and livestock (Ruddiman 2005). That influence significantly increased after the industrial revolution (from 1769 to 1840), and it has further increased with an accelerating growth rate since then. The Earth's population rose from 1 billion in 1800 to more than 7.8 billion in 2021, which was associated with a significant global-scale economic expansion. One of the consequences is the rising greenhouse gas emissions (e.g., carbon dioxide, CO_2, nitrous oxide, N_2O, and methane, CH_4), which are directly related to global warming.

The atmospheric CO_2 levels and land surface temperature are related to melting glaciers and sea ice. In the present paper, as noted by Castle and Hendry (2020, Chapter 6), we name the climate econometric models of those variables as ice-age models. During the 4.5 billion-year history of the Earth, the variables ice volume, atmospheric CO_2, and land surface temperature simultaneously changed, driven by exogenous orbital variables, such as (i) changes in the non-circularity of the Earth's orbit with a period of 100 thousand years, (ii) changes in the tilt of the Earth's rotational axis relative to the ecliptic (i.e., the plane of the Earth's orbit around the Sun) with a period of 41 thousand years, and (iii) circular rotation of the rotational axis itself,

which changes the season at which the Earth's orbit is nearest to the Sun, with a period that is between 19 to 23 thousand years (it is variable due to the changes in the tilt of the rotational axis). The orbital variables are exogenous to humanity, and in this paper we disentangle them from the effects of humanity on the Earth's climate in the statistical inferences. In addition to the aforementioned orbital variables, other exogenous variables which also influence the Earth's climate are the following: variations in the Sun's radiation output, volcanic eruption particles in the atmosphere and ice cover, and changes in the magnetic poles (Castle and Hendry 2020).

As in the work of Castle and Hendry (2020), we use data for climate and orbital variables for the last 798 thousand-year period, and we provide out-of-sample forecasts of Antarctic ice volume, atmospheric CO_2, and land surface temperature for the last 100 thousand years. Those authors use the automatic model selection method named Autometrics (Doornik 2009), to approximate the unknown data generating process (DGP) of climate data. They also motivate the application of econometric techniques to study climate change, by referring to the similar time series properties of the economic and climate data (e.g., non-stationarity, non-linearity, stochastic seasonality, and extreme observations).

In this paper, we also use the model selection results of Castle and Hendry (2020), with respect to the order of the dependent variables in the ice-age models, selection of the orbital variables affecting the insolation of the Earth, parameter restrictions, and lag-order selection of the dependent and explanatory variables. We study the robustness of the results of the above authors, and we improve their model specification by considering more general score-driven updates in the measurement and transition equations of the ice-age model. In this way, we improve the dynamic specification of the benchmark ice-age model (Castle and Hendry 2020).

Score-driven time series models are introduced in the works of Creal et al. (2008) and Harvey and Chakravarty (2008). Those models are generalizations of classical time series models, for example, ARMA (autoregressive moving average) (Box and Jenkins 1970), and GARCH (generalized autoregressive conditional heteroskedasticity) (Engle 1982; Bollerslev 1986). Score-driven models are robust to outliers and missing observations (Harvey 2013), and a score-driven

update, asymptotically at the true values of parameters, reduces the Kullback–Leibler distance between the score-driven filter and the true DGP in every step (Blasques et al. 2015).

These advantages of the score-driven models motivate their application to climate data. We compare the statistical and forecasting performances of the ice-age model of Castle and Hendry (2020) with those of our score-driven ice-age models. The likelihood-based model performance metrics and diagnostic tests of this paper indicate that the climate econometric model of Castle and Hendry (2020) is improved. We report impulse responses among Antarctic ice volume, atmospheric CO_2 level, and land surface temperature, which are robust for the ice-age model of Castle and Hendry (2020) and all score-driven ice-age models of the present paper.

By using data for the first 698 thousand years of the sample (for which humanity did not influence the Earth's climate), we present out-of-sample forecasts of the Antarctic ice volume, atmospheric CO_2 level, and land surface temperature for the period of the last 100 thousand years of the sample. We find that the forecasting results of Castle and Hendry (2020) are robust. For the last 10-15 thousand years when humanity influenced the Earth's climate, we find that: (i) the forecasts of ice volume are above the observed ice volume, (ii) the forecasts of the atmospheric CO_2 level are below the observed CO_2 level, and (iii) the forecasts of temperature are below the observed temperature. For the last 20 thousand years of the sample, the new score-driven homoskedastic ice-age model for the t-distribution provides the best forecasting performance for all variables. The results disentangle the effects of humanity and the effects of the exogenous variables on the Earth's climate, and motivate to take further actions to achieve the "very low greenhouse gas emissions scenario" (Intergovernmental Panel on Climate Change, 2021).

The remainder of this paper is organized as follows: Section 2 presents the econometric methods. Section 3 presents the data and the empirical results. Section 4 presents the discussion.

2. Climate Econometrics

2.1. Benchmark Ace-Age Model

Model specification—In the work of Castle and Hendry (2020, Chapter 6), estimation and forecasting results are presented for a general unrestricted model (GUM), named the ice-age model.

That model specification is the benchmark model of the present paper. We study the robustness of the results for the ice-age model, and extend the model specification by using score-driven dynamics. In this section, we review the benchmark ice-age model of Castle and Hendry (2020).

The dependent variables y_t (3×1) of the ice-age model are $y_t = (\text{Ice}_t, \text{CO}_t, \text{Temp}_t)'$, where 'Ice' denotes Antarctic ice volume, 'CO_2' denotes atmospheric carbon dioxide level, and 'Temp' denotes Antarctic-based land surface temperature. The order of the variables in y_t is defined in the work of Castle and Hendry (2020), which we use for all models of the present paper. Correspondingly, the ice-age model is specified as follows:

$$y_t = \mu_t + v_t = \gamma_0 + \Gamma_1 y_{t-1} + \Gamma_2 z_t + \Gamma_3 z_{t-1} + v_t \tag{1}$$

where μ_t (3×1) is the conditional mean of y_t given $\mathcal{F}_{t-1} \equiv \sigma(y_1, \ldots, y_{t-1}, z_1, \ldots, z_t)$, the reduced-form error term $v_t \sim N_3(0_{3\times1}, \Sigma)$ has a multivariate i.i.d. normal distribution, where the covariance matrix is $\Sigma \equiv \Omega\Omega'$ (3×3), for which Ω (3×3) is a lower-triangular matrix with positive elements in the diagonal, and z_t (9×1) includes strongly exogenous explanatory variables (Castle and Hendry 2020). We initialize μ_t by using the start values of the dependent variables y_1. We assume that the maximum modulus of the eigenvalues of Γ_1, denoted as C_μ, is less than one.

The elements of the vector of explanatory variables z_t are three main interacting orbital changes over time affecting solar radiation that could drive ice ages (Castle and Hendry 2020):

$$z_t = (\text{Ec}_t, \text{Ob}_t, \text{Pr}_t, \text{Ec}_t \times \text{Ob}_t, \text{Ec}_t \times \text{Pr}_t, \text{Ob}_t \times \text{Pr}_t, \text{Ec}_t^2, \text{Ob}_t^2, \text{Pr}_t^2)' \tag{2}$$

where 'Ec' measures the eccentricity (i.e., non-circularity) of the Earth's orbit, 'Ob' is obliquity measuring the tilt of the Earth's rotational axis relative to the ecliptic, and 'Pr' is a measure of the precession of the equinox (i.e., circular rotation of the rotational axis itself).

The conditional mean μ_t in Equation (1) includes the vector of constant parameters γ_0 (3×1), and parameter matrices Γ_1 (3×3), Γ_2 (3×9), and Γ_3 (3×9). We note that the more general GUM formulation of Castle and Hendry (2020, p. 102) includes the vector of dummy variables

of outliers, which are not included in the estimated GUM specifications of Castle and Hendry (2020, p. 104). For the benchmark ice-age model, we report estimation and forecasting results for Equation (1) which excludes the outlier-dummies. The same outlier-dummies are also excluded from the score-driven ice-age models of the present paper, because those models are robust to extreme observations (Harvey 2013).

The GUM estimates reported in the work of Castle and Hendry (2020, p. 104) impose restrictions on the matrices Γ_1, Γ_2, and Γ_3. According to those restrictions, the following elements of Γ_1 are not restricted to zero: $\Gamma_{1,1,1}$, $\Gamma_{1,1,3}$, $\Gamma_{1,2,2}$, $\Gamma_{1,2,3}$, $\Gamma_{1,3,2}$, and $\Gamma_{1,3,3}$. The following elements of Γ_2 are not restricted to zero: $\Gamma_{2,1,1}$, $\Gamma_{2,1,4}$, $\Gamma_{2,1,5}$, $\Gamma_{2,2,1}$, $\Gamma_{2,2,7}$, $\Gamma_{2,3,1}$, $\Gamma_{2,3,4}$, and $\Gamma_{2,3,5}$. Furthermore, the following elements of Γ_3 are also not restricted to zero: $\Gamma_{3,1,1}$, $\Gamma_{3,1,2}$, $\Gamma_{3,1,4}$, $\Gamma_{3,2,1}$, $\Gamma_{3,2,2}$, $\Gamma_{3,2,4}$, and $\Gamma_{3,3,4}$. The benchmark ice-age model is estimated by using the maximum likelihood (ML) method, as in the work of Castle and Hendry (2020).

Impulse responses—We estimate the dynamic effects of the i.i.d. structural-form error term $\epsilon_t \equiv \Omega^{-1} v_t \sim N_3(0_{3\times 1}, I_3)$. The corresponding IRFs are defined as follows:

$$\frac{\partial y_{t+j}}{\partial \epsilon_t} = \Gamma_1^j \Omega \quad \text{for} \quad j = 0, \ldots, \infty \tag{3}$$

The IRFs are identified by using the sign restrictions for the contemporaneous effects among the elements of v_t, which is based on simulations of matrix Ω, according to the following procedure (Rubio-Ramirez et al. 2010): First, the ML estimates of Ω are used. Second, a $K \times K$ matrix $\tilde{K}$ of independent $N(0,1)$ numbers is simulated. For the IRFs, 3 million simulations of $\tilde{K}$ are generated, only those simulations are used that satisfy the sign restrictions, and for each simulation Ω is replaced by $\tilde{\Omega}$ in the IRF formulas. For the simulations that satisfy the sign restrictions, we report the mean $\pm$ one standard deviation estimates of the IRFs. Third, the QR decomposition (Rubio-Ramirez et al. 2010) of $\tilde{K}$ is performed, and the resulting matrices are denoted as $\tilde{Q}$ (orthogonal matrix) and $\tilde{R}$ (upper triangular matrix). Fourth, we define $\tilde{\Omega} \equiv \Omega \times \tilde{Q}'$. For each simulation of $\tilde{\Omega}$, sign restrictions are used in accordance with Table 1.

The sign restrictions of Table 1 are motivated as follows: (i) In the work of Castle and Hendry (2020, Tables 6.2 and 6.3), the correlation coefficient estimates among the residuals of the ice-age model are reported. The sign restrictions in Table 1 are according to the correlation coefficients of Castle and Hendry (2020). (ii) For the negative effects of CO_2 on Ice_t, and for the positive effects of Ice_t on Temp_t of Table 1, we refer to the work of Qin and Buehler (2012). For the positive interaction effects between CO_2 and Temp_t of Table 1, we also refer to the works of Jouzel et al. (2007) and Lüthi et al. (2008). (iii) For the negative effects of Ice_t on CO_2 of Table 1, we refer to the work of Wadham et al. (2019). (iv) For the positive effects of Temp_t on CO_2 of Table 1, we refer to the work of Archer et al. (2004). (v) For the negative interaction effects between Temp_t and Ice_t of Table 1, we refer to the work of Bronselaer et al. (2018).

Table 1. Sign restrictions on contemporaneous impact responses.

	Ice_t shock	$\text{CO}_{2,t}$ shock	Temp_t shock
Ice_t	+	−	−
$\text{CO}_{2,t}$	−	+	+
Temp_t	−	+	+

2.2. Score-Driven Ice-Age Models

2.2.1. Score-Driven Homoskedastic Ice-Age Model

Model specification—The score-driven ice-age model of this paper uses the score-driven model specification in the work of Harvey (2013, p. 56). The model is specified as follows:

$$y_t = \mu_t + v_t \tag{4}$$

$$\mu_t = \gamma_0 + \Gamma_1 \mu_{t-1} + \Gamma_2 z_t + \Gamma_3 z_{t-1} + \Psi u_{t-1} \tag{5}$$

where μ_t (3×1) is the conditional mean of y_t given $\mathcal{F}_{t-1} \equiv \sigma(y_1, \ldots, y_{t-1}, z_1, \ldots, z_t, \mu_1)$, v_t is the multivariate i.i.d. reduced-form error term, z_t (9×1) is the vector of strongly exogenous explanatory variables, and u_t (3×1) is the vector of scaled score functions (Harvey 2013). The assumption of strict exogeneity of z_t is from the work of Harvey (2013, p. 56), which is

supported for z_t of Equation (2) in the work of Castle and Hendry (2020, p. 95). We initialize μ_t by using the start values of the dependent variables y_1 (Harvey 2013). The conditional mean μ_t includes the following parameters: the vector of constant parameters γ_0 (3×1), and the parameter matrices Γ_1 (3×3), Γ_2 (3×9), Γ_3 (3×9), and Ψ (3×3). We assume that the maximum modulus of the eigenvalues of Γ_1, denoted as C_μ, is less than one.

For Γ_1, Γ_2, and Γ_3, we use the same aforementioned restrictions as in the work of Castle and Hendry (2020), which is motivated by the following general-to-specific model selection procedure. In the first step, for the parameter estimation of the score-driven ice-age model, we start with the aforementioned restrictions of Γ_2 and Γ_3, and initially we use unrestricted parameter matrices for Γ_1 and Ψ. In a second step, we restrict those parameters of Γ_1 and Ψ to zero which are not significant at the 1% level. In this way, the same elements of Γ_1 and Ψ are restricted for the score-driven models as for matrix Γ_1 in the work of Castle and Hendry (2020). Hence, the following elements of Ψ are not restricted to zero: $\Psi_{1,1}$, $\Psi_{1,3}$, $\Psi_{2,2}$, $\Psi_{2,3}$, $\Psi_{3,2}$, and $\Psi_{3,3}$.

The reduced-form error term $v_t \sim t_3(0, \Sigma, \nu)$ has a multivariate i.i.d. t-distribution, where the scale matrix is $\Sigma \equiv \Omega\Omega'$ (3×3), for which Ω (3×3) is a lower-triangular squared matrix with positive elements in the diagonal, and $\nu > 2$ is the degrees of freedom parameter (the restriction on the parameter space $\nu > 2$ ensures that the covariance matrix of v_t is well-defined).

The scaled score function u_t is defined as follows. The log of the conditional density of y_t is:

$$\ln f(y_t|\mathcal{F}_{t-1};\Theta) = \ln\Gamma\left(\frac{\nu+3}{2}\right) - \ln\Gamma\left(\frac{\nu}{2}\right) - \frac{3}{2}\ln(\pi\nu) \tag{6}$$

$$-\frac{1}{2}\ln|\Sigma| - \frac{\nu+3}{2}\ln\left[1 + \frac{v_t'\Sigma^{-1}v_t}{\nu}\right]$$

where $v_t = y_t - \mu_t$, $\Theta = (\Theta_1, \ldots, \Theta_S)'$ is the vector of time-invariant parameters, which includes the elements of γ_0, Γ_1, Γ_2, Γ_3, Ψ, Ω, and ν. The partial derivative of the log conditional density $\ln f(y_t|\mathcal{F}_{t-1};\Theta)$ with respect to μ_t is (Harvey 2013):

$$\frac{\partial \ln f(y_t|\mathcal{F}_{t-1};\Theta)}{\partial \mu_t} = \frac{\nu+3}{\nu}\Sigma^{-1} \times \left(1 + \frac{v_t'\Sigma^{-1}v_t}{\nu}\right)^{-1} v_t \equiv \frac{\nu+3}{\nu}\Sigma^{-1} \times u_t \tag{7}$$

The scaled score function u_t is defined in the second equality of Equation (7), where v_t is multiplied by $[1+(v_t'\Sigma^{-1}v_t)/\nu]^{-1} = \nu/(\nu+v_t'\Sigma^{-1}v_t) \in (0,1)$. Therefore, the scaled score function is bounded by the reduced-form error term: $|u_t| < |v_t|$. All elements of u_t are bounded functions of v_t for $\nu < \infty$ (Harvey 2013), hence all moments of u_t are well-defined. In the work of Harvey (2013), it is shown that u_t is multivariate i.i.d. with mean zero and a covariance matrix:

$$\text{Var}(u_t) = E\left[\frac{\partial \ln f(y_t|\mathcal{F}_{t-1};\Theta)}{\partial \mu_t} \times \frac{\partial \ln f(y_t|\mathcal{F}_{t-1};\Theta)}{\partial \mu_t'}\right] = \frac{\nu+3}{\nu+5} \times \Sigma^{-1} \tag{8}$$

We also note that if $\nu \to \infty$, then $u_t \to_p v_t$. In the limiting case, Equations (3) and (4) provide a VARMAX(1,1) (vector autoregressive moving average with exogenous variables, VARMAX) structure for the dependent variables:

$$y_t = \gamma_0 + \Gamma_1 y_{t-1} + \Gamma_2 z_t + \Gamma_3 z_{t-1} + (\Psi - \Gamma_1)v_{t-1} + v_t \tag{9}$$

The benchmark ice-age model is a special case of the score-driven ice-age model, because if $\nu \to \infty$ and $\Psi = \Gamma_1$ for Equations (4) and (5), then we obtain Equation (1). This can also be seen for the limiting case for $\nu \to \infty$ in Equation (9), by using $\Psi = \Gamma_1$. We name Equation (9) the score-driven homoskedastic Gaussian ice-age model.

All score-driven models are estimated by using the maximum likelihood (ML) method (Harvey 2013; Blasques et al. 2021). For the ML estimation, we assume correct model specifications for all econometric models of the present paper. Under that assumption, the standard errors of the ML estimates are consistently estimated by using the outer product of the gradient of the log-likelihood (LL) function. Another consequence of the correct model specification assumption is that the updating terms of the score-driven filters, asymptotically and at the true values of parameters, are white noise vectors. For technical details on the statistical inference of score-driven models, we refer to the works of Harvey and Chakravarty (2008), Harvey (2013), Creal et al. (2008, 2011, 2013), Blasques et al. (2021), and Blazsek et al. (2020, 2021a, 2021b).

Impulse responses—First, we define the vector of the structural-form error terms ϵ_t (3×1).

The variance of the reduced-form error term $v_t \sim t_3(0, \Sigma, \nu)$ is factorized, as follows:

$$\text{Var}(v_t) = \Sigma \times \frac{\nu}{\nu - 2} = \left(\frac{\nu}{\nu - 2}\right)^{1/2} \times \Omega\Omega' \times \left(\frac{\nu}{\nu - 2}\right)^{1/2} \tag{10}$$

Based on that, the following multivariate i.i.d. structural-form error term ϵ_t is introduced:

$$v_t = \left(\frac{\nu}{\nu - 2}\right)^{1/2} \Omega \times \epsilon_t \tag{11}$$

where $E(\epsilon_t) = 0$, $\text{Var}(\epsilon_t) = I_3$ and $\epsilon_t \sim t_3[0, I_3 \times (\nu - 2)/\nu, \nu]$. Furthermore, by substituting Equation (11) into Equation (7), u_t as a function of the structural-form error term is:

$$u_t = [(\nu - 2)\nu]^{1/2} \Omega \frac{\epsilon_t}{\nu - 2 + \epsilon_t' \epsilon_t}. \tag{12}$$

Second, from Equations (4) and (5), the nonlinear MA(∞) representation of y_t is:

$$y_t = v_t + \sum_{j=0}^{\infty} \left(\Gamma_1^j \gamma_0 + \Gamma_1^j \Gamma_2 z_{t-j} + \Gamma_1^j \Gamma_3 z_{t-1-j} + \Gamma_1^j \Psi u_{t-1-j}\right) \tag{13}$$

$$= \left(\frac{\nu}{\nu - 2}\right)^{1/2} \Omega \times \epsilon_t$$

$$+ \sum_{j=0}^{\infty} \left\{ \phi^j \gamma_0 + \Gamma_1^j \Gamma_2 z_{t-j} + \Gamma_1^j \Gamma_3 z_{t-1-j} + \Gamma_1^j \Psi [(\nu - 2)\nu]^{1/2} \Omega \frac{\epsilon_{t-1-j}}{\nu - 2 + \epsilon_{t-1-j}' \epsilon_{t-1-j}} \right\}$$

We focus on the impulse responses for the dependent variables y_t, because the variables within z_t are strongly exogenous to humanity. From y_t, we are particularly interested in the dynamic effects of the atmospheric carbon dioxide level on the Antarctic-based land surface temperature, because humanity has influence on the CO_2 emissions. Thus, the new measurement method of impulse responses for the score-driven ice-age model of this paper may have policy implications in relation to carbon dioxide emissions regulation. The contemporaneous and dynamic effects

of the structural-form error term ϵ_t, respectively, are given by the following equations:

$$\frac{\partial y_t}{\partial \epsilon_t} = \left(\frac{\nu}{\nu-2}\right)^{1/2} \Omega \tag{14}$$

$$\frac{\partial y_{t+j}}{\partial \epsilon_t} = \Gamma_1^{j-1} \Psi [(\nu-2)\nu]^{1/2} \Omega \tilde{D}_t \quad \text{for} \quad j = 1, \ldots, \infty \tag{15}$$

where

$$\tilde{D}_t = \begin{bmatrix} \frac{\nu-2+\epsilon_t'\epsilon_t-2\epsilon_{1,t}^2}{(\nu-2+\epsilon_t'\epsilon_t)^2} & \frac{-2\epsilon_{1,t}\epsilon_{2,t}}{(\nu-2+\epsilon_t'\epsilon_t)^2} & \frac{-2\epsilon_{1,t}\epsilon_{3,t}}{(\nu-2+\epsilon_t'\epsilon_t)^2} \\ \frac{-2\epsilon_{2,t}\epsilon_{1,t}}{(\nu-2+\epsilon_t'\epsilon_t)^2} & \frac{\nu-2+\epsilon_t'\epsilon_t-2\epsilon_{2,t}^2}{(\nu-2+\epsilon_t'\epsilon_t)^2} & \frac{-2\epsilon_{2,t}\epsilon_{3,t}}{(\nu-2+\epsilon_t'\epsilon_t)^2} \\ \frac{-2\epsilon_{3,t}\epsilon_{1,t}}{(\nu-2+\epsilon_t'\epsilon_t)^2} & \frac{-2\epsilon_{3,t}\epsilon_{2,t}}{(\nu-2+\epsilon_t'\epsilon_t)^2} & \frac{\nu-2+\epsilon_t'\epsilon_t-2\epsilon_{3,t}^2}{(\nu-2+\epsilon_t'\epsilon_t)^2} \end{bmatrix} \tag{16}$$

We note that IRFs for the ice-age model are not reported in the work of Castle and Hendry (2020). We study the robustness of the results of Castle and Hendry (2020), by comparing the IRFs of the score-driven ice-age models and the IRFs of the benchmark ice-age model.

In Equation (15), the dynamic interaction effects are time-dependent due to $\tilde{D}_t$. In the empirical applications of the present paper we replace $\tilde{D}_t$ by the sample average (White 2001) for the last 10 observations of the sample, because, as noted in the work of Castle and Hendry (2020, p. 111), humanity has influenced climate for the last 10 thousand years. There are alternative ways for the estimation of dynamic interaction effects for nonlinear models (Lütkepohl 2005), hence the IRF estimation of our paper may be modified in future applications.

Finally, we also report contemporaneous and dynamic effects of the structural-form error term ϵ_t for the score-driven ice-age model for the multivariate normal distribution:

$$\frac{\partial y_t}{\partial \epsilon_t} = \Omega \tag{17}$$

$$\frac{\partial y_{t+j}}{\partial \epsilon_t} = \Gamma_1^{j-1} \Psi \Omega \quad \text{for} \quad j = 1, \ldots, \infty \tag{18}$$

The IRFs of this section are identified by using the procedure of Rubio-Ramirez et al. (2010).

2.2.2. Score-Driven Heteroskedastic Ice-Age Model

Model specification—We extend the score-driven ice-age model for the homoskedastic multi-

variate t-distribution, by considering score-driven conditional heteroskedasticity with constant correlation coefficients for the reduced form error term v_t. The model is specified as follows:

$$y_t = \mu_t + v_t \tag{19}$$

$$\mu_t = \gamma_0 + \Gamma_1 \mu_{t-1} + \Gamma_2 z_t + \Gamma_3 z_{t-1} + \Psi u_{t-1} \tag{20}$$

where μ_t (3×1) is the conditional mean of y_t given $\mathcal{F}_{t-1}$, which is defined later in this section, v_t is the multivariate i.i.d. reduced-form error term, z_t (9×1) is the vector of strongly exogenous explanatory variables, and u_t (3×1) is the vector of scaled score functions. We initialize μ_t by using y_1 (Harvey 2013). The conditional mean μ_t includes includes the following parameters: the vector of constant parameters γ_0 (3×1), and the parameter matrices Γ_1 (3×3), Γ_2 (3×9), Γ_3 (3×9), and Ψ (3×3). For the parameters of μ_t, we use the same restrictions as for the homoskedastic score-driven ice-age model for the t-distribution. We assume that the maximum modulus of the eigenvalues of Γ_1, denoted as C_μ, is less than one.

The reduced-form error term $v_t|(\mathcal{F}_{t-1}; \Theta) \sim t_3(0, \Sigma_t, \nu)$ has a multivariate conditional t-distribution, where degrees of freedom $\nu > 2$, the scale matrix is $\Sigma_t \equiv D_t R D_t$, where D_t (3×3) is a time-varying diagonal matrix with the score-driven scales of each time series, and R (3×3) is the time-invariant correlation matrix. The specification of this section assumes that the correlation coefficients are constant over time. This specification can be extended according to the results of Creal et al. (2011) to dynamic correlation coefficients, by using a score-driven volatility plus correlation model for the t-distribution.

The positive definiteness of R and boundedness of the correlation coefficients for $(-1, 1)$ are ensured by using the following specification: $R = \Delta^{-1} Q \Delta^{-1} \equiv \Delta^{-1} \Omega \Omega' \Delta^{-1}$, where Δ (3×3) is a diagonal matrix in which the elements of the diagonal are the square roots of the elements of the diagonal of the positive definite matrix Q (3×3) (Engle 2002). The positive definiteness of Q is ensured by using the Cholesky decomposition $Q = \Omega \Omega'$, in which Ω (3×3) is a lower triangular matrix with positive elements in the diagonal. For parameter identification reasons,

each element of the diagonal of Ω is restricted to one. Furthermore, D_t is specified as follows:

$$D_t = \begin{bmatrix} \exp(\lambda_{1,t}) & 0 & 0 \\ 0 & \exp(\lambda_{2,t}) & 0 \\ 0 & 0 & \exp(\lambda_{3,t}) \end{bmatrix} \tag{21}$$

We specify the filters $\lambda_{i,t}$ in Equation (21) as follows:

$$\lambda_{i,t} = \omega_i + \beta_i \lambda_{i,t} + \alpha_i e_{i,t-1} + \alpha_i^* \text{sgn}(-v_{i,t-1})(e_{i,t-1} + 1) \tag{22}$$

where $\text{sgn}(\cdot)$ is the signum function, and α_i^* for $i = 1, 2, 3$ measure asymmetric effects in the conditional scale of the dependent variables. We initialize $\lambda_{i,t}$ for $i = 1, 2, 3$ using the unconditional mean $E(\lambda_{i,t}) = \omega_i/(1 - \beta_i)$ for $i = 1, 2, 3$, respectively (Harvey 2013). In the following, we define the updating terms u_t and $e_{i,t}$. For the covariance stationarity of $\lambda_{i,t}$, asymptotically at the true values of parameters, it is required that $C_{i,\lambda} = |\beta_i| < 1$ for $i = 1, 2, 3$.

First, the scaled score function u_t is defined as follows. The log conditional density of y_t is:

$$\ln f(y_t|\mathcal{F}_{t-1}; \Theta) = \ln \Gamma\left(\frac{\nu+3}{2}\right) - \ln \Gamma\left(\frac{\nu}{2}\right) - \frac{3}{2}\ln(\pi\nu) \tag{23}$$

$$-\frac{1}{2}\ln|\Sigma_t| - \frac{\nu+3}{2}\ln\left[1 + \frac{v_t'\Sigma_t^{-1}v_t}{\nu}\right]$$

where $v_t = y_t - \mu_t$, $\mathcal{F}_{t-1} \equiv \sigma(y_1, \ldots, y_{t-1}, z_1, \ldots, z_t, \mu_1, \lambda_{1,1}, \lambda_{2,1}, \lambda_{3,1})$, $\Theta = (\Theta_1, \ldots, \Theta_S)'$ is the vector of time-invariant parameters, which includes the elements of γ_0, Γ_1, Γ_2, Γ_3, Ψ, Ω, ω_1, ω_2, ω_3, β_1, β_2, β_3, α_1, α_2, α_3, α_1^*, α_2^*, α_3^*, and ν. The partial derivative of the log of the conditional density $\ln f(y_t|\mathcal{F}_{t-1}; \Theta)$ with respect to μ_t is:

$$\frac{\partial \ln f(y_t|\mathcal{F}_{t-1}; \Theta)}{\partial \mu_t} = \frac{\nu+3}{\nu}\Sigma_t^{-1} \times \left(1 + \frac{v_t'\Sigma_t^{-1}v_t}{\nu}\right)^{-1} v_t \equiv \frac{\nu+3}{\nu}\Sigma_t^{-1} \times u_t \tag{24}$$

The scaled score function u_t is defined in the second equality of Equation (24), where v_t is

multiplied by $[1 + (v_t'\Sigma_t^{-1}v_t)/\nu]^{-1} = \nu/(\nu + v_t'\Sigma_t^{-1}v_t) \in (0,1)$. Therefore, the scaled score function is bounded by the reduced-form error term: $|u_t| < |v_t|$. All elements of u_t are bounded functions of v_t for $\nu < \infty$, hence all moments of u_t are well-defined. The scaled score function $u_t|(\mathcal{F}_{t-1};\Theta)$ has a zero conditional mean and the following conditional covariance matrix:

$$\mathrm{Var}(u_t|\mathcal{F}_{t-1};\Theta) = \frac{\nu+3}{\nu+5} \times \Sigma_t^{-1} \tag{25}$$

The latter result is an extension of the work of Harvey (2013, p. 206).

Second, the updating term $e_{i,t}$ for $i = 1,2,3$ is defined as follows. The conditional distributions of the marginals of y_t are $y_{i,t}|(\mathcal{F}_{t-1};\Theta) \sim t[\mu_{i,t}, \exp(\lambda_{i,t}), \nu]$ for $i = 1,2,3$ (Kibria and Joarder 2006). The log of the conditional density of $y_{i,t}|(\mathcal{F}_{t-1};\Theta)$ for $i = 1,2,3$ is

$$\ln f_i(y_{i,t}|\mathcal{F}_{t-1};\Theta) = \ln\Gamma\left(\frac{\nu+1}{2}\right) - \ln\Gamma\left(\frac{\nu}{2}\right) - \frac{1}{2}\ln(\pi\nu) - \lambda_{i,t} \tag{26}$$

$$-\frac{\nu+1}{2}\ln\left[1 + \frac{v_{i,t}^2}{\nu\exp(2\lambda_{i,t})}\right]$$

where $v_{i,t} = y_{i,t} - \mu_{i,t}$. We define the updating term of the filter $\lambda_{i,t}$ for $i = 1,2,3$ as follows:

$$e_{i,t} \equiv \frac{\partial \ln f_i(v_{i,t}|\mathcal{F}_{t-1};\Theta)}{\partial\lambda_{i,t}} = \frac{(\nu+1)v_{i,t}^2}{\nu\exp(2\lambda_{i,t}) + v_{i,t}^2} - 1 \tag{27}$$

Equations (22) and (27) are the Beta-t-EGARCH with leverage effects model of Harvey and Chakravarty (2008) (see also Creal et al. 2013 and Harvey 2013).

Impulse responses—First, we define the structural-form error terms ϵ_t (3×1). The conditional variance of the reduced-form error term $v_t|(\mathcal{F}_{t-1};\Theta) \sim t_3(0,\Sigma_t,\nu)$ is factorized, as follows:

$$\mathrm{Var}(v_t|\mathcal{F}_{t-1};\Theta) = \Sigma_t \times \frac{\nu}{\nu-2} = \left(\frac{\nu}{\nu-2}\right)^{1/2} D_t\Delta^{-1}\Omega \times \Omega'\Delta^{-1}D_t\left(\frac{\nu}{\nu-2}\right)^{1/2} \tag{28}$$

Based on that, the following multivariate i.i.d. structural-form error term ϵ_t is introduced:

$$v_t = \left(\frac{\nu}{\nu-2}\right)^{1/2} D_t \Delta^{-1} \Omega \times \epsilon_t \tag{29}$$

where $E(\epsilon_t) = 0$, $\text{Var}(\epsilon_t) = I_3$ and $\epsilon_t \sim t_3[0, I_3 \times (\nu-2)/\nu, \nu]$. Furthermore, by substituting Equation (29) into Equation (24), u_t as a function of the structural-form error term is:

$$u_t = [(\nu-2)\nu]^{1/2} D_t \Delta^{-1} \Omega \frac{\epsilon_t}{\nu - 2 + \epsilon_t' \epsilon_t}. \tag{30}$$

Second, from Equations (19) and (20), the nonlinear MA(∞) representation of y_t is:

$$y_t = v_t + \sum_{j=0}^{\infty} \left(\Gamma_1^j \gamma_0 + \Gamma_1^j \Gamma_2 z_{t-j} + \Gamma_1^j \Gamma_3 z_{t-1-j} + \Gamma_1^j \Psi u_{t-1-j}\right) \tag{31}$$

$$= \left(\frac{\nu}{\nu-2}\right)^{1/2} D_t \Delta^{-1} \Omega \times \epsilon_t$$

$$+ \sum_{j=0}^{\infty} \left\{ \phi^j \gamma_0 + \Gamma_1^j \Gamma_2 z_{t-j} + \Gamma_1^j \Gamma_3 z_{t-1-j} + \Gamma_1^j \Psi [(\nu-2)\nu]^{1/2} D_t \Delta^{-1} \Omega \frac{\epsilon_{t-1-j}}{\nu - 2 + \epsilon_{t-1-j}' \epsilon_{t-1-j}} \right\}$$

The contemporaneous and dynamic effects of the structural-form error term ϵ_t, respectively, are given by the following equations:

$$\frac{\partial y_t}{\partial \epsilon_t} = \left(\frac{\nu}{\nu-2}\right)^{1/2} D_t \Delta^{-1} \Omega \tag{32}$$

$$\frac{\partial y_{t+j}}{\partial \epsilon_t} = \Gamma_1^{j-1} \Psi [(\nu-2)\nu]^{1/2} D_t \Delta^{-1} \Omega \tilde{D}_t \quad \text{for} \quad j = 1, \ldots, \infty \tag{33}$$

where $\tilde{D}_t$ is given by Equation (16). In Equations (32) and (33), the dynamic interaction effects are time-dependent due to D_t and $\tilde{D}_t$. We replace D_t and $\tilde{D}_t$ by their sample averages for the last 10 observations of the sample (Castle and Hendry 2020). The IRFs are identified by using the procedure of Rubio-Ramirez et al. (2010). We also refer to the work of Lütkepohl (2005) for alternative estimation methods for time-varying IRFs.

3. Empirical Results

3.1. Data and In-Sample Results

Data—In Table 2, the dependent and the explanatory variables are presented. The table shows the definition of each variable, observation period, units of measurement, data sources, and some descriptive statistics. In Figures 1 and 2, the evolution of the dependent and explanatory variables, respectively, are presented. According to Figures 1(b) and 1(c), atmospheric $CO_{2,t}$ and land surface temperature Temp_t, respectively, remarkably are in unison. In Figure 1, it can also be noticed that Antarctic ice volume Ice_t moves in the opposite direction from $CO_{2,t}$ and Temp_t, creating the ice-age and inter-glacial periods periodically. The seasonality of the dependent variables (Figure 1), which is partly due to the three main interacting orbital changes over time affecting solar radiation (Figure 2), is clearly observed in these figures.

In-sample results—In Table 3, the ML parameter estimates for the (i) benchmark ice-age model (Castle and Hendry 2020), (ii) score-driven homoskedastic ice-age model for the normal distribution, (iii) score-driven homoskedastic ice-age model for the t-distribution, and (iv) score-driven heteroskedastic ice-age model for the t-distribution are reported. According to the table, under the parameter restrictions for Γ_1, Γ_2, Γ_3, and Ψ, the estimated parameters, for all models, are significantly different from zero. For the most general score-driven heteroskedastic ice-age model for the t-distribution, significant and asymmetric volatility dynamics are estimated, as α_i and β_i for $i = 1, 2, 3$, and α_i^* for $i = 1, 2$, are significantly different from zero.

In Table 4, the statistical performance metrics and some diagnostic test results for the models of Table 3 are reported. The statistical performances are compared by using the LL, Akaike information criterion (AIC), Bayesian information criterion (BIC), and Hannan–Quinn criterion (HQC) metrics. The use of these variables for score-driven models is motivated by the work of Harvey (2013, p. 56). We find that the statistical performance of the score-driven heteroskedastic ice-age model for the t-distribution is superior to the statistical performances of other specifications of Tables 3 and 4. For all models, we find that the C_μ and $C_{i,\lambda}$ for $i = 1, 2, 3$ statistics support the covariance stationarity of μ_t and $\lambda_{i,t}$, respectively. As a diagnostic test of

the residuals, we use the Ljung–Box test (Ljung and Box 1978) for all elements of v_t, ϵ_t, u_t, and e_t. The diagnostic tests for the score functions u_t, and e_t are motivated by the work of Harvey (2013, p. 55), due to the robustness to extreme observations of the score-function-based Ljung–Box test. The Ljung–Box test results indicate that the ice-age model of Castle and Hendry (2020) is not fully supported, which is noted in the same work (p. 102, footnote 4). From the score-driven ice-age specifications, full support is provided for the most general score-driven heteroskedastic ice-age model for the t-distribution.

In the following, we present the parameter estimates for the benchmark ice-age model (Equation (1)) and the score-driven heteroskedastic ice-age model for the t-distribution (Equation (20)). First, the estimates of Equation (1) are given by (Table 3):

$$\begin{aligned}\hat{\text{Ice}}_t &= 1.3735 + 0.8549\ \text{Ice}_{t-1} - 0.0208\ \text{Temp}_{t-1} + 95.8353\ \text{Ec}_t - 47.5937\ \text{Ec}_t\text{Ob}_t \\ &\quad -5.2167\ \text{Ec}_t\text{Pr}_t - 93.5393\ \text{Ec}_{t-1} - 0.3706\ \text{Ob}_{t-1} + 46.7753\ \text{Ec}_{t-1}\text{Ob}_{t-1}\end{aligned} \tag{34}$$

$$\begin{aligned}\hat{\text{CO}}_{2,t} &= 1.8718 + 0.8468\ \text{CO}_{2,t-1} + 0.0136\ \text{Temp}_{t-1} + 13.8095\ \text{Ec}_t + 0.2106\ \text{Ob}_t^2 \\ &\quad -27.1270\ \text{Ec}_{t-1} - 1.1138\ \text{Ob}_{t-1} + 5.6423\ \text{Ec}_{t-1}\text{Ob}_{t-1}\end{aligned} \tag{35}$$

$$\begin{aligned}\hat{\text{Temp}}_t &= -2.6657 + 0.8587\ \text{CO}_{2,t-1} + 0.8684\ \text{Temp}_{t-1} - 335.9696\ \text{Ec}_t \\ &\quad +254.2055\ \text{Ec}_t\text{Ob}_t + 26.6287\ \text{Ec}_t\text{Pr}_t - 111.3537\ \text{Ec}_{t-1}\text{Ob}_{t-1}\end{aligned} \tag{36}$$

The estimates correspond to the estimates of Castle and Hendry (2020, p. 104). We note that one unit of $\text{CO}_{2,t}$ is 7.8 gigatonnes in their work, and one unit of $\text{CO}_{2,t}$ is 780 gigatonnes in the present paper. Hence, the difference between the $\text{CO}_{2,t}$ parameter estimates in their work (p. 104, Equation (6.4)), and our $\text{CO}_{2,t}$ parameter estimates. Second, the estimates of Equation (20) are given by (Table 3):

$$\begin{aligned}\hat{\text{Ice}}_t &= 1.1817 + 0.8824\ \text{Ice}_{t-1} - 0.0172\ \text{Temp}_{t-1} + 84.6136\ \text{Ec}_t - 42.7119\ \text{Ec}_t\text{Ob}_t \\ &\quad -4.8681\ \text{Ec}_t\text{Pr}_t - 83.4944\ \text{Ec}_{t-1} - 0.3307\ \text{Ob}_{t-1} + 42.4409\ \text{Ec}_{t-1}\text{Ob}_{t-1} \\ &\quad +0.9651\ u_{1,t-1} - 0.0289\ u_{3,t-1}\end{aligned} \tag{37}$$

$$\begin{aligned}\hat{\mathrm{CO}}_{2,t} &= 1.4068 + 0.8528\ \mathrm{CO}_{2,t-1} + 0.0122\ \mathrm{Temp}_{t-1} + 11.9581\ \mathrm{Ec}_t + 0.1270\ \mathrm{Ob}_t^2 \\ &\quad -26.3809\ \mathrm{Ec}_{t-1} - 0.7289\ \mathrm{Ob}_{t-1} + 6.1482\ \mathrm{Ec}_{t-1}\mathrm{Ob}_{t-1} \\ &\quad +1.3943\ u_{2,t-1} + 0.0166\ u_{3,t-1}\end{aligned} \tag{38}$$

$$\begin{aligned}\hat{\mathrm{Temp}}_t &= -0.6955 + 0.1382\ \mathrm{CO}_{2,t-1} + 0.9377\ \mathrm{Temp}_{t-1} - 272.0190\ \mathrm{Ec}_t \\ &\quad +194.7069\ \mathrm{Ec}_t\mathrm{Ob}_t + 17.5525\ \mathrm{Ec}_t\mathrm{Pr}_t - 78.4289\ \mathrm{Ec}_{t-1}\mathrm{Ob}_{t-1} \\ &\quad +4.7059\ u_{2,t-1} + 0.9860\ u_{3,t-1}\end{aligned} \tag{39}$$

To compare the parameter estimates of Equations (34)-(36) with those of Equations (37)-(39), the dynamic interaction effects for Antarctic ice volume, atmospheric CO_2, and land surface temperature are studied by using the IRFs.

In Figures 3 to 6, the IRFs for the (i) benchmark ice-age model, (ii) score-driven homoskedastic ice-age model for the normal distribution, (iii) score-driven homoskedastic ice-age model for the t-distribution, and (iv) score-driven heteroskedastic ice-age model for the t-distribution, respectively, are reported. The IRF estimates for the score-driven models indicate robust IRF estimation results in the work of Castle and Hendry (2020). The IRFs of Figures 3 to 6 are identified by using sign restrictions on the contemporaneous relations. The IRF figures indicate that the signs of the dynamic interaction effects are coherent with the signs of the same interaction effects of the aforementioned works of Archer et al. (2004), Jouzel et al. (2007), Lüthi et al. (2008), Qin and Buehler (2012), Bronselaer et al. (2018), Wadham et al. (2019), and Castle and Hendry (2020). According to Figures 3 to 6, the IRF estimates are persistent and are consistent with the estimates of the long-run solutions of Equation (1) reported in the work of Castle and Hendry (2020, p. 107, Table 6.4).

By comparing the IRF estimates of the benchmark ice-age model with those of the score-driven ice-age models, for several panels of Figures 3 to 6, stronger effects are measured for the score-driven ice-age models than for the benchmark ice-age model. The strongest effects are measured for the score-driven heteroskedastic ice-age model for the t-distribution (Figure 6). We find the following differences: (i) For the benchmark ice-age model, the dynamic effects of

a unit Ice_t shock (i.e., measured based on the δ^{18}O proxy) on $\text{CO}_{2,t}$ are less than -0.25 (i.e., -195 gigatonnes of CO_2), while for the score-driven models the same effect is stronger and it is approximately -0.35 (i.e., -273 gigatonnes of CO_2) (Figures 3 to 6, Panel (d)). (ii) For the benchmark ice-age model, the dynamic effects of a unit Temp_t shock on $\text{CO}_{2,t}$ are less than 0.25 (i.e., 195 gigatonnes of CO_2), while for the score-driven models the same effect is stronger, and it is between 0.30 and 0.35 (i.e., 234 and 273 gigatonnes of CO_2, respectively) (Figures 3 to 6, Panel (f)). (iii) For the benchmark ice-age model, the dynamic effects of a unit Ice_t shock (i.e., measured based on the δ^{18}O proxy) on Temp_t are less than -0.35 (i.e., -3.5 Celsius degrees), while for the score-driven models the same effect is stronger, reaching an estimate between -0.40 and -0.45 (i.e., -4 and -4.5 Celsius degrees, respectively) (Figures 3 to 6, Panel (g)). (iv) For the benchmark ice-age model, the dynamic effects of a unit $\text{CO}_{2,t}$ shock (i.e., an increase of 780 gigatonnes of CO_2 in the atmosphere) on Temp_t is approximately 3.5 Celsius degrees, while it is above 4 Celsius degrees for the score-driven ice-age models (Figures 3 to 6, Panel (h)).

Finally, in Figure 7, we present the scaled score function u_t as a function of the structural-form error term ϵ_t. The figure presents the estimates for the score-driven heteroskedastic ice-age model for the t-distribution, which is the best-performing ice-age specification according to the likelihood-based model selection metrics. In the three-dimensional graphs of Figure 7, we present the elements of u_t from Equation (30) as functions of $\epsilon_{1,t}$ and $\epsilon_{2,t}$, where $\epsilon_{3,t} = 0$ for the purpose of illustration. We note that within the D_t term of Equation (30), we use the unconditional mean estimate of $\lambda_{i,t}$ for $i = 1, 2, 3$, which is $\hat{E}(\lambda_{i,t}) = \hat{\omega}_i/(1-\hat{\beta}_i)$ for $i = 1, 2, 3$, respectively. The figure indicates that extreme values of the structural-form error terms are discounted by the scaled score functions. This supports the outlier-robustness of the score-driven ice-age models of the present paper. We also note that very similar score-functions are estimated for the score-driven homoskedastic ice-age model for the t-distribution.

Table 2. Descriptive statistics.

(a) Dependent variables	Ice_t	$\text{CO}_{2,t}$	Temp_t
Variable	Ice volume	Atmospheric CO_2	Antarctic-based land surface temperature
Start date	798 thousand years ago	798 thousand years ago	798 thousand years ago
End date	1 thousand years ago	1 thousand years ago	1 thousand years ago
Data frequency	1 thousand years	1 thousand years	1 thousand years
Measurement	Based on the δ^{18}O proxy	1 unit = 780 gigatonnes of CO_2	1 unit = 1 Celsius degree
Data source	Lisiecki and Raymo (2005)	Lüthi et al. (2008)	Jouzel et al. (2007)
Sample size	798	798	798
Minimum	3.1000	1.7269	−10.2530
Maximum	5.0800	2.9500	3.7662
Mean	4.1707	2.2382	−5.2892
Standard deviation	0.4467	0.2546	2.9009

(b) Explanatory variables	Ec_t	Ob_t	Pr_t
Variable	Eccentricity of the Earth's orbit	Obliquity	Precession of the equinox
Start date	798 thousand years ago	798 thousand years ago	798 thousand years ago
End date	1 thousand years ago	1 thousand years ago	1 thousand years ago
Data frequency	1 thousand years	1 thousand years	1 thousand years
Measurement	Periodicity deriving from the changing non-circularity of the Earth's orbit (zero denotes circularity).	Periodicity deriving from the changes in the tilt of the Earth's rotational axis relative to the ecliptic (1 unit = 10 degrees).	Periodicity deriving from the precession of the equinox (1 unit = 1 degree).
Data source	Paillard et al. (1996)	Paillard et al. (1996)	Paillard et al. (1996)
Sample size	798	798	798
Minimum	0.0042	2.2076	0.0008
Maximum	0.0500	2.4455	0.3593
Mean	0.0271	2.3342	0.1802
Standard deviation	0.0119	0.0591	0.1039

(a). Ice volume Ice_t

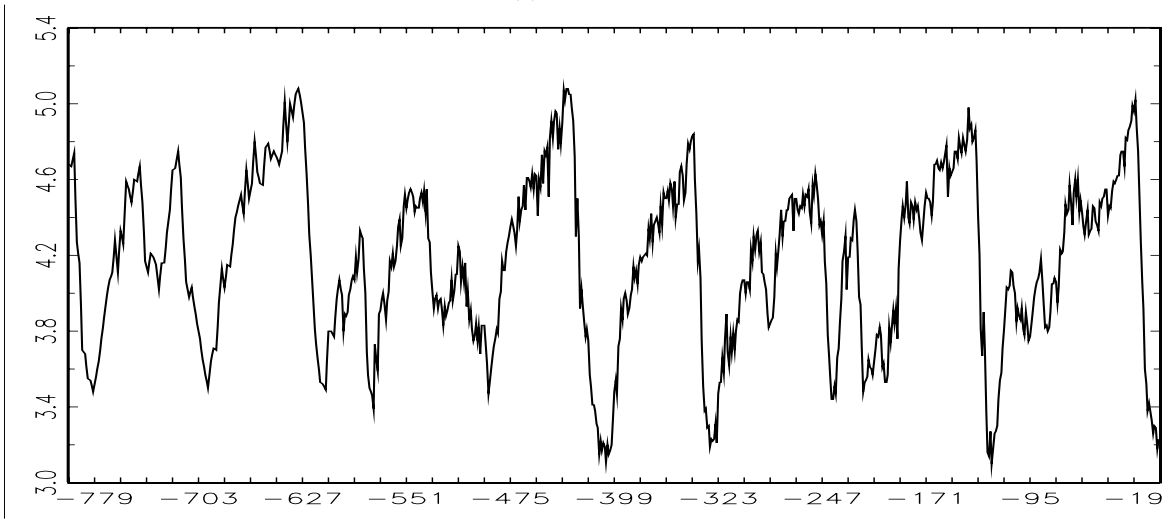

(b). Atmospheric carbon dioxide level $\text{CO}_{2,t}$

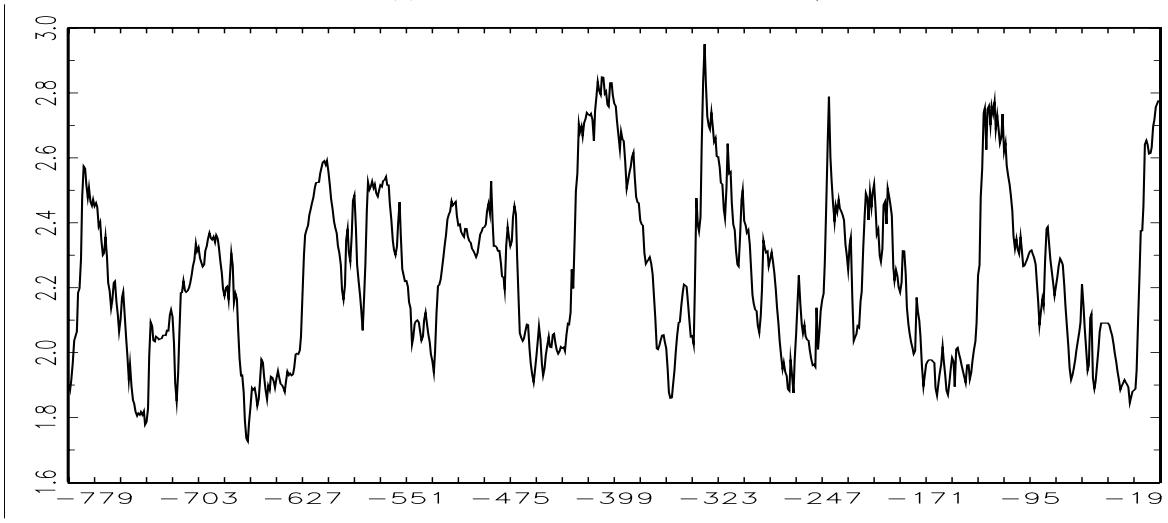

(c). Antarctic-based land surface temperature Temp_t

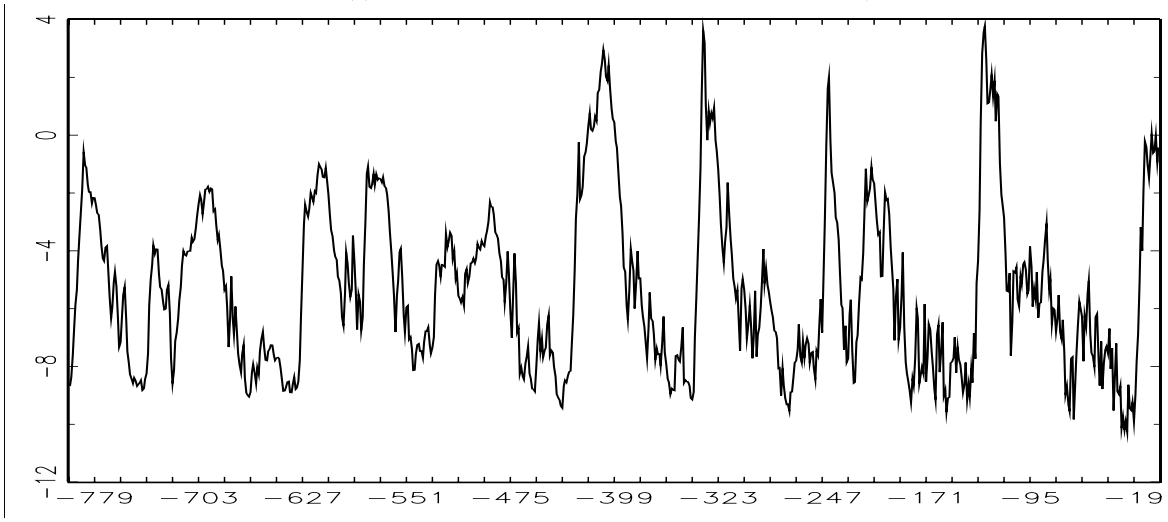

Figure 1. Evolution of Ice_t, $\text{CO}_{2,t}$, and Temp_t from 798 thousand years ago to 1 thousand years ago.

(a). Eccentricity of the Earth's orbit Ec_t

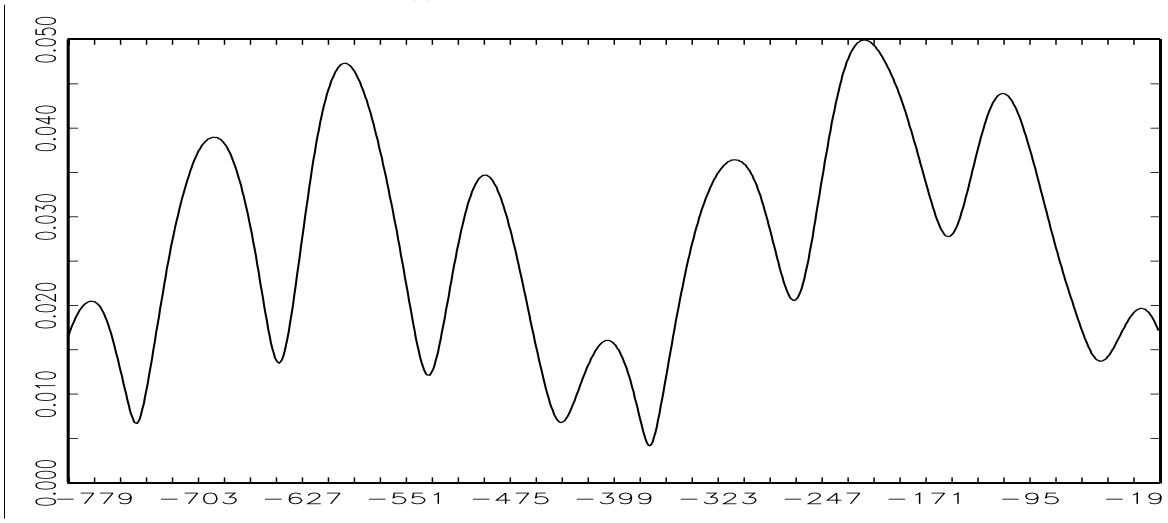

(b). Obliquity (the tilt of the Earth's rotational axis relative to the ecliptic) Ob_t

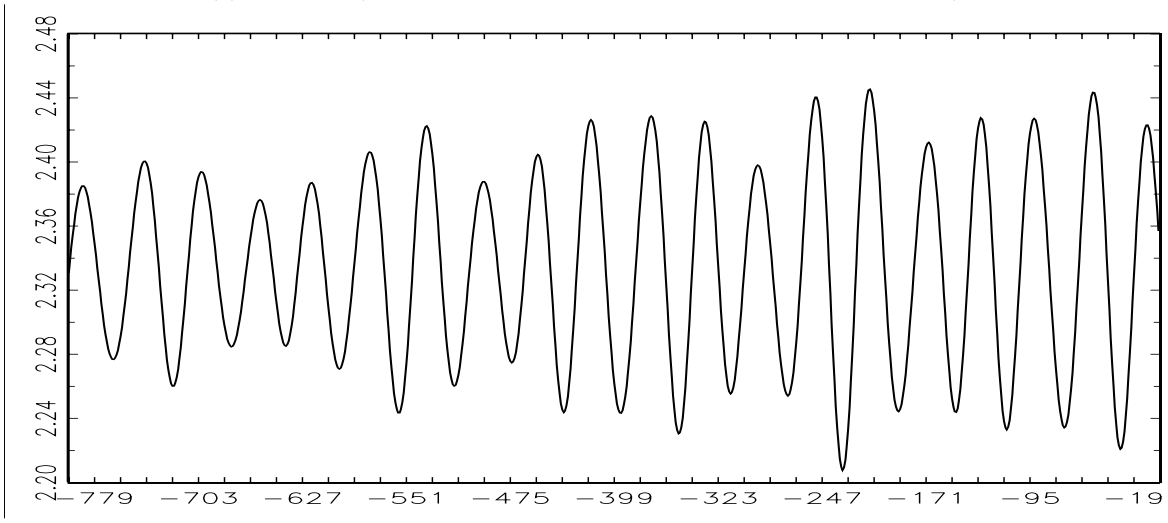

(c). Precession of the equinox (circular rotation of the rotational axis itself) Pr_t

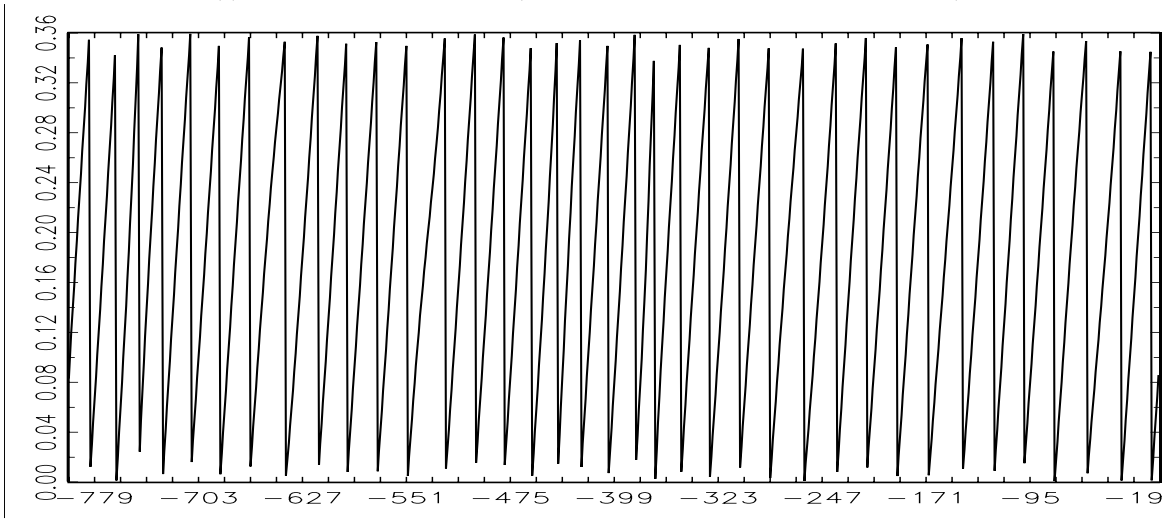

Figure 2. Evolution of Ec_t, Ob_t, and Pr_t from 798 thousand years ago to 1 thousand years ago.

Table 3. In-sample ML parameter estimates.

Benchmark ice-age model		Score-driven homoskedastic Gaussian ice-age model		Score-driven homoskedastic t ice-age model		Score-driven heteroskedastic t ice-age model			
$\gamma_{0,1}$	1.3735***(0.3009)	$\gamma_{0,1}$	1.2697***(0.2884)	$\gamma_{0,1}$	1.2745***(0.2798)	$\gamma_{0,1}$	1.1817***(0.2812)	ω_1	−1.1773***(0.2845)
$\gamma_{0,2}$	1.8718***(0.3023)	$\gamma_{0,2}$	1.6589***(0.3552)	$\gamma_{0,2}$	1.8197***(0.3579)	$\gamma_{0,2}$	1.4068***(0.3259)	ω_2	−0.7409***(0.1416)
$\gamma_{0,3}$	−2.6657***(0.6905)	$\gamma_{0,3}$	−1.4256^{+}(0.9049)	$\gamma_{0,3}$	−1.4366^{+}(0.9252)	$\gamma_{0,3}$	−0.6955(0.6592)	ω_3	−0.0455***(0.0139)
$\Gamma_{1,1,1}$	0.8549***(0.0144)	$\Gamma_{1,1,1}$	0.8733***(0.0155)	$\Gamma_{1,1,1}$	0.8738***(0.0150)	$\Gamma_{1,1,1}$	0.8824***(0.0162)	β_1	0.5266***(0.1144)
$\Gamma_{1,1,3}$	−0.0208***(0.0020)	$\Gamma_{1,1,3}$	−0.0175***(0.0024)	$\Gamma_{1,1,3}$	−0.0175***(0.0024)	$\Gamma_{1,1,3}$	−0.0172***(0.0025)	β_2	0.7628***(0.0446)
$\Gamma_{1,2,2}$	0.8468***(0.0176)	$\Gamma_{1,2,2}$	0.8410***(0.0287)	$\Gamma_{1,2,2}$	0.8291***(0.0286)	$\Gamma_{1,2,2}$	0.8528***(0.0231)	β_3	0.8796***(0.0286)
$\Gamma_{1,2,3}$	0.0136***(0.0016)	$\Gamma_{1,2,3}$	0.0125***(0.0026)	$\Gamma_{1,2,3}$	0.0137***(0.0026)	$\Gamma_{1,2,3}$	0.0122***(0.0022)	α_1	0.0500***(0.0192)
$\Gamma_{1,3,2}$	0.8587***(0.2556)	$\Gamma_{1,3,2}$	0.3714(0.3333)	$\Gamma_{1,3,2}$	0.3771(0.3396)	$\Gamma_{1,3,2}$	0.1382(0.2458)	α_2	0.0930***(0.0154)
$\Gamma_{1,3,3}$	0.8684***(0.0231)	$\Gamma_{1,3,3}$	0.9008***(0.0297)	$\Gamma_{1,3,3}$	0.8995***(0.0304)	$\Gamma_{1,3,3}$	0.9377***(0.0228)	α_3	0.1070***(0.0172)
$\Gamma_{2,1,1}$	95.8353***(30.3012)	$\Gamma_{2,1,1}$	88.7529***(29.2107)	$\Gamma_{2,1,1}$	88.1550***(28.6783)	$\Gamma_{2,1,1}$	84.6136***(28.7107)	α_1^*	0.0513***(0.0163)
$\Gamma_{2,1,4}$	−47.5937***(12.4804)	$\Gamma_{2,1,4}$	−45.5349***(12.0258)	$\Gamma_{2,1,4}$	−45.9952***(11.8462)	$\Gamma_{2,1,4}$	−42.7119***(12.0538)	α_2^*	−0.0199^{+}(0.0124)
$\Gamma_{2,1,5}$	−5.2167***(1.0663)	$\Gamma_{2,1,5}$	−5.4569***(1.0321)	$\Gamma_{2,1,5}$	−5.6132***(1.0064)	$\Gamma_{2,1,5}$	−4.8681***(0.9172)	α_3^*	−0.0094(0.0123)
$\Gamma_{2,2,1}$	13.8095***(3.8487)	$\Gamma_{2,2,1}$	14.5128***(4.8910)	$\Gamma_{2,2,1}$	14.8536***(4.8133)	$\Gamma_{2,2,1}$	11.9581***(3.5543)		
$\Gamma_{2,2,7}$	0.2106***(0.0446)	$\Gamma_{2,2,7}$	0.1688***(0.0518)	$\Gamma_{2,2,7}$	0.1876***(0.0515)	$\Gamma_{2,2,7}$	0.1270***(0.0477)		
$\Gamma_{2,3,1}$	−335.9696***(38.6135)	$\Gamma_{2,3,1}$	−311.6342***(43.7423)	$\Gamma_{2,3,1}$	−326.4885***(44.2197)	$\Gamma_{2,3,1}$	−272.0190***(32.9400)		
$\Gamma_{2,3,4}$	254.2055***(28.4900)	$\Gamma_{2,3,4}$	240.1468***(30.8981)	$\Gamma_{2,3,4}$	258.2711***(30.4240)	$\Gamma_{2,3,4}$	194.7069***(22.0173)		
$\Gamma_{2,3,5}$	26.6287***(8.3118)	$\Gamma_{2,3,5}$	25.0557***(7.8012)	$\Gamma_{2,3,5}$	28.2720***(7.6689)	$\Gamma_{2,3,5}$	17.5525***(5.9466)		
$\Gamma_{3,1,1}$	−93.5393***(31.3704)	$\Gamma_{3,1,1}$	−83.6310***(30.7764)	$\Gamma_{3,1,1}$	−81.9865***(30.4458)	$\Gamma_{3,1,1}$	−83.4944***(30.2589)		
$\Gamma_{3,1,2}$	−0.3706***(0.1233)	$\Gamma_{3,1,2}$	−0.3519***(0.1164)	$\Gamma_{3,1,2}$	−0.3544***(0.1131)	$\Gamma_{3,1,2}$	−0.3307***(0.1135)		
$\Gamma_{3,1,4}$	46.7753***(12.9406)	$\Gamma_{3,1,4}$	43.5364***(12.6666)	$\Gamma_{3,1,4}$	43.5483***(12.5889)	$\Gamma_{3,1,4}$	42.4409***(12.6434)		
$\Gamma_{3,2,1}$	−27.1270***(6.7356)	$\Gamma_{3,2,1}$	−29.1279***(7.5563)	$\Gamma_{3,2,1}$	−30.6263***(7.4143)	$\Gamma_{3,2,1}$	−26.3809***(6.1789)		
$\Gamma_{3,2,2}$	−1.1138***(0.2191)	$\Gamma_{3,2,2}$	−0.9235***(0.2529)	$\Gamma_{3,2,2}$	−1.0217***(0.2528)	$\Gamma_{3,2,2}$	−0.7289***(0.2339)		
$\Gamma_{3,2,4}$	5.6423**(2.2875)	$\Gamma_{3,2,4}$	6.2517**(2.4809)	$\Gamma_{3,2,4}$	6.7580***(2.4337)	$\Gamma_{3,2,4}$	6.1482***(2.1916)		
$\Gamma_{3,3,4}$	−111.3537***(24.0465)	$\Gamma_{3,3,4}$	−107.2597***(26.1398)	$\Gamma_{3,3,4}$	−119.1342***(26.2451)	$\Gamma_{3,3,4}$	−78.4289***(16.6672)		
$\Psi_{1,1,1}$	NA	$\Psi_{1,1,1}$	0.7982***(0.0343)	$\Psi_{1,1,1}$	0.9020***(0.0438)	$\Psi_{1,1,1}$	0.9651***(0.0551)		
$\Psi_{1,1,3}$	NA	$\Psi_{1,1,3}$	−0.0295***(0.0041)	$\Psi_{1,1,3}$	−0.0325***(0.0050)	$\Psi_{1,1,3}$	−0.0289***(0.0047)		
$\Psi_{1,2,2}$	NA	$\Psi_{1,2,2}$	1.1351***(0.0300)	$\Psi_{1,2,2}$	1.3418***(0.0545)	$\Psi_{1,2,2}$	1.3943***(0.0599)		
$\Psi_{1,2,3}$	NA	$\Psi_{1,2,3}$	0.0197***(0.0025)	$\Psi_{1,2,3}$	0.0221***(0.0030)	$\Psi_{1,2,3}$	0.0166***(0.0025)		
$\Psi_{1,3,2}$	NA	$\Psi_{1,3,2}$	4.1436***(0.5376)	$\Psi_{1,3,2}$	4.9368***(0.7038)	$\Psi_{1,3,2}$	4.7059***(0.6182)		
$\Psi_{1,3,3}$	NA	$\Psi_{1,3,3}$	0.8723***(0.0347)	$\Psi_{1,3,3}$	1.0084***(0.0480)	$\Psi_{1,3,3}$	0.9860***(0.0538)		
$\Omega_{1,1}$	0.0891***(0.0019)	$\Omega_{1,1}$	0.0887***(0.0019)	$\Omega_{1,1}$	0.0861***(0.0021)	$\Omega_{1,1}$	NA		
$\Omega_{2,1}$	−0.0102***(0.0018)	$\Omega_{2,1}$	−0.0085***(0.0018)	$\Omega_{2,1}$	−0.0096***(0.0018)	$\Omega_{2,1}$	−0.1698***(0.0410)		
$\Omega_{2,2}$	0.0524***(0.0011)	$\Omega_{2,2}$	0.0492***(0.0010)	$\Omega_{2,2}$	0.0475***(0.0010)	$\Omega_{2,2}$	NA		
$\Omega_{3,1}$	−0.1755***(0.0267)	$\Omega_{3,1}$	−0.1600***(0.0262)	$\Omega_{3,1}$	−0.1672***(0.0274)	$\Omega_{3,1}$	−0.2343***(0.0449)		
$\Omega_{3,2}$	0.3808***(0.0249)	$\Omega_{3,2}$	0.3440***(0.0239)	$\Omega_{3,2}$	0.3476***(0.0247)	$\Omega_{3,2}$	0.5107***(0.0424)		
$\Omega_{3,3}$	0.6711***(0.0145)	$\Omega_{3,3}$	0.6684***(0.0146)	$\Omega_{3,3}$	0.6458***(0.0152)	$\Omega_{3,3}$	NA		
ν	NA	ν	NA	ν	38.2860***(6.1464)	ν	27.7970***(5.1586)		

Notes: Not available (NA). Standard errors are reported in parentheses. ***, **, *, and $^{+}$ indicate significance at the 1%, 5%, 10%, and 15% levels, respectively.

Table 4. Model performance and diagnostics for in-sample estimates.

	Benchmark ice-age model	Score-driven homoskedastic Gaussian ice-age model	Score-driven homoskedastic t ice-age model	Score-driven heteroskedastic t ice-age model
LL	1.5094	1.5801	1.6026	1.7644
AIC	−2.9435	−3.0699	−3.1126	−3.4134
BIC	−2.7675	−2.8587	−2.8955	−3.1435
HQC	−2.8759	−2.9887	−3.0291	−3.3097
C_μ	0.9663	0.9453	0.9444	0.9543
$C_{\lambda,1}$	NA	NA	NA	0.5266
$C_{\lambda,2}$	NA	NA	NA	0.7628
$C_{\lambda,3}$	NA	NA	NA	0.8796
LB $v_{1,t}$ (p-value)	20.5200(0.8448)	17.8671(0.9294)	19.1502(0.8934)	19.3022(0.8886)
LB $v_{2,t}$ (p-value)	118.9560***(0.0000)	28.4522(0.4407)	29.2620(0.3993)	30.8129(0.3255)
LB $v_{3,t}$ (p-value)	41.8520**(0.0448)	30.2398(0.3518)	33.0351(0.2345)	37.1410(0.1158)
LB $\epsilon_{1,t}$ (p-value)	20.5200(0.8448)	17.8671(0.9294)	19.1502(0.8934)	16.9958(0.9487)
LB $\epsilon_{2,t}$ (p-value)	98.1577***(0.0000)	28.6594(0.4300)	27.1411(0.5106)	21.1773(0.8179)
LB $\epsilon_{3,t}$ (p-value)	47.0696**(0.0135)	44.3814**(0.0255)	45.6695**(0.0189)	33.1683(0.2296)
LB $u_{1,t}$ (p-value)	NA	NA	19.9979(0.8645)	21.7319(0.7935)
LB $u_{2,t}$ (p-value)	NA	NA	27.8256(0.4737)	27.7605(0.4772)
LB $u_{3,t}$ (p-value)	NA	NA	33.5007(0.2178)	35.0719(0.1678)
LB $e_{1,t}$ (p-value)	NA	NA	NA	34.1775(0.1951)
LB $e_{2,t}$ (p-value)	NA	NA	NA	25.8774(0.5798)
LB $e_{3,t}$ (p-value)	NA	NA	NA	22.7776(0.7441)

Notes: Not available (NA); log-likelihood (LL); Akaike information criterion (AIC); Bayesian information criterion (BIC); Hannan–Quinn criterion (HQC); Ljung–Box (LB). C_μ is the maximum modulus of eigenvalues of the matrix Γ_1, for which $C_1 < 1$ indicates covariance stationarity of the location filter. $C_{\lambda,i} = |\beta_i|$ for $i = 1, 2, 3$, for which $C_{\lambda,i} < 1$ for $i = 1, 2, 3$ indicates covariance stationarity of the scale filter. The lag-order for the LB test is $28 \simeq \sqrt{T}$. *** and ** indicate significance at the 1% and 5% levels, respectively.

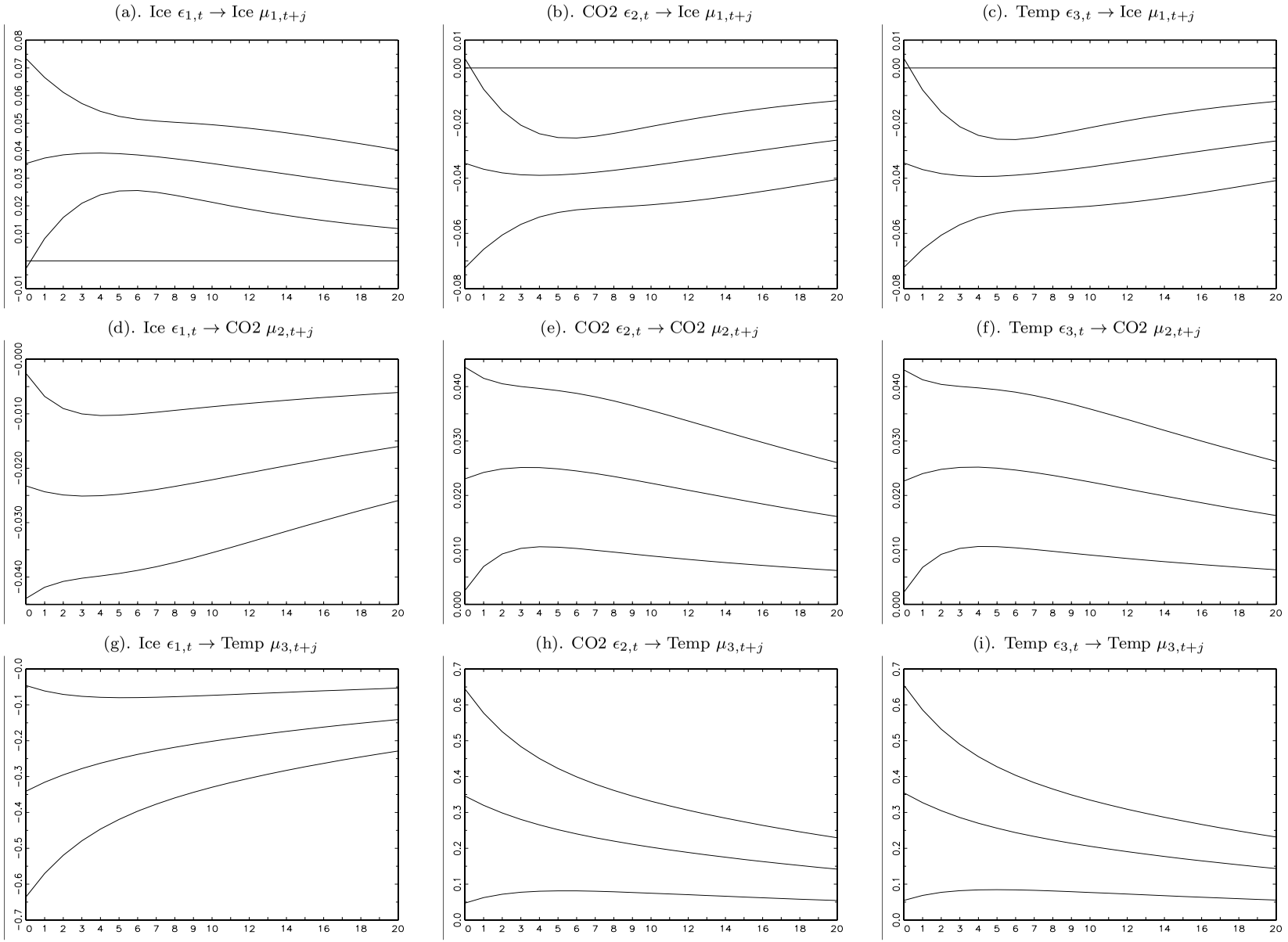

Figure 3. IRFs for the benchmark ice-age model (Castle and Hendry 2020).

Notes: The confidence interval is mean ± one standard deviation that is estimated for 2,302 out of the 3 million simulations, for which the restrictions of Table 1 are satisfied.

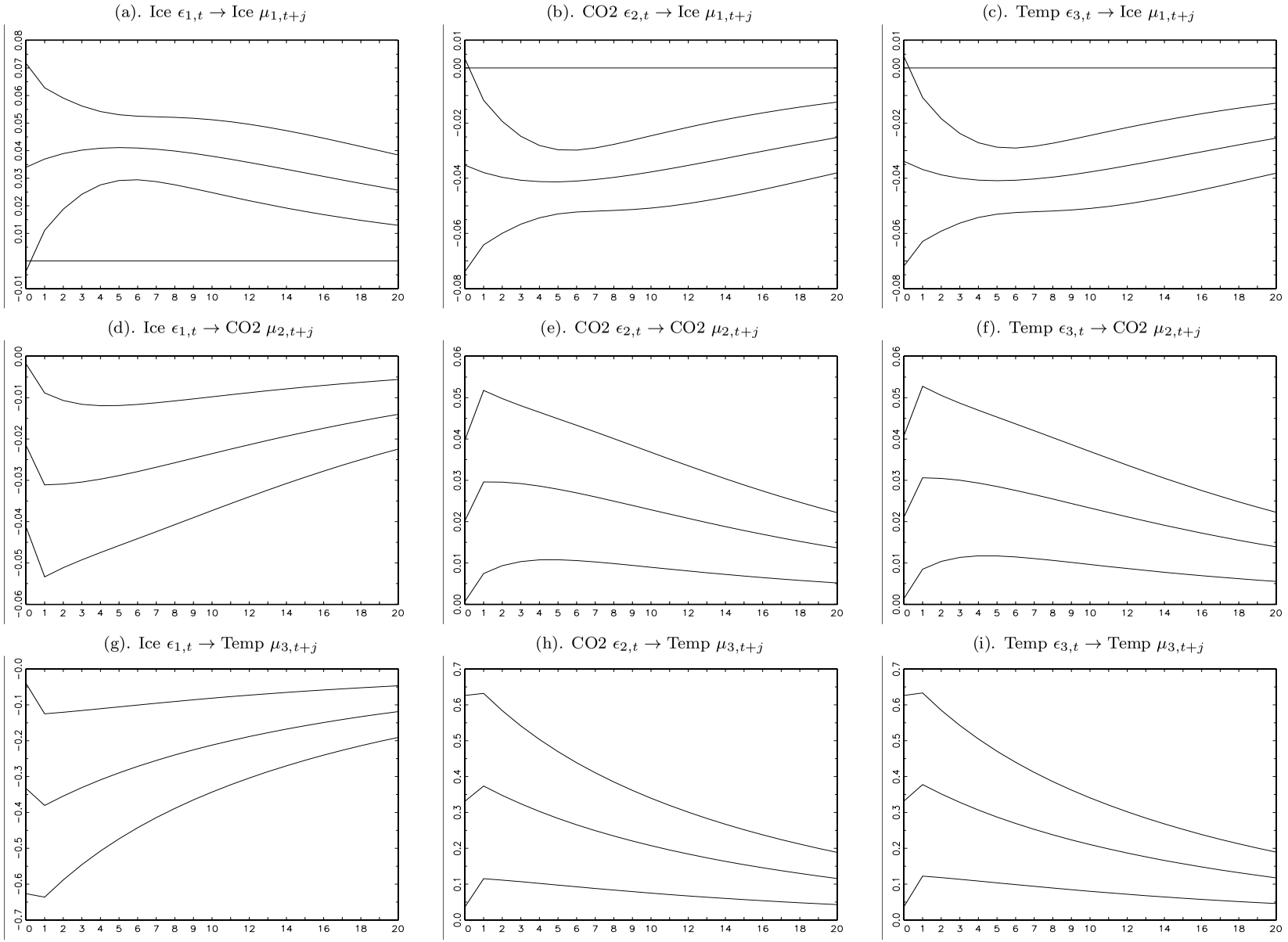

Figure 4. IRFs for the score-driven ice-age model for the normal distribution.

Notes: The confidence interval is mean ± one standard deviation that is estimated for 1,771 out of the 3 million simulations, for which the restrictions of Table 1 are satisfied.

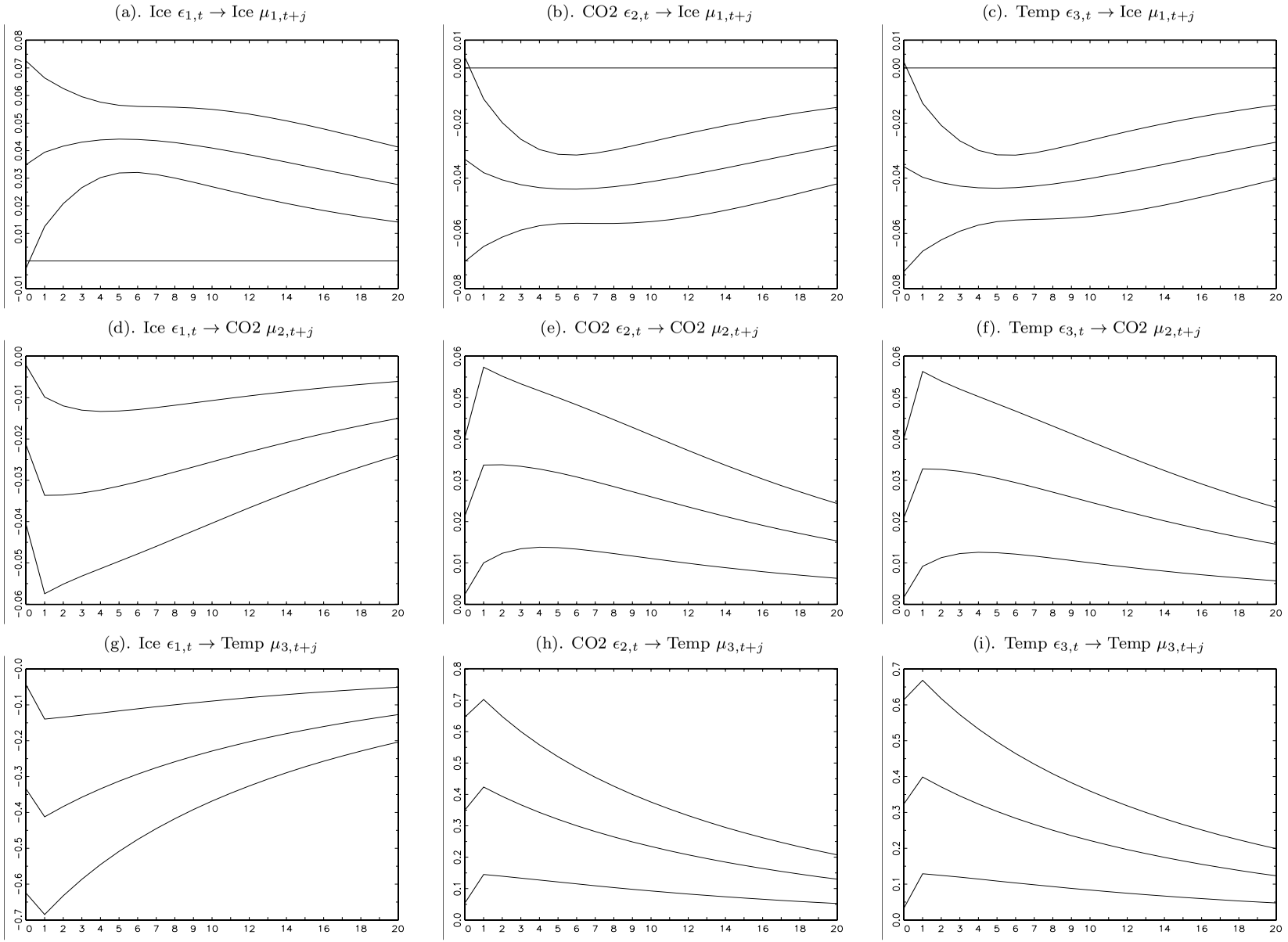

Figure 5. IRFs for the score-driven homoskedastic ice-age model for the t-distribution.

Notes: The confidence interval is mean ± one standard deviation that is estimated for 2,289 out of the 3 million simulations, for which the restrictions of Table 1 are satisfied.

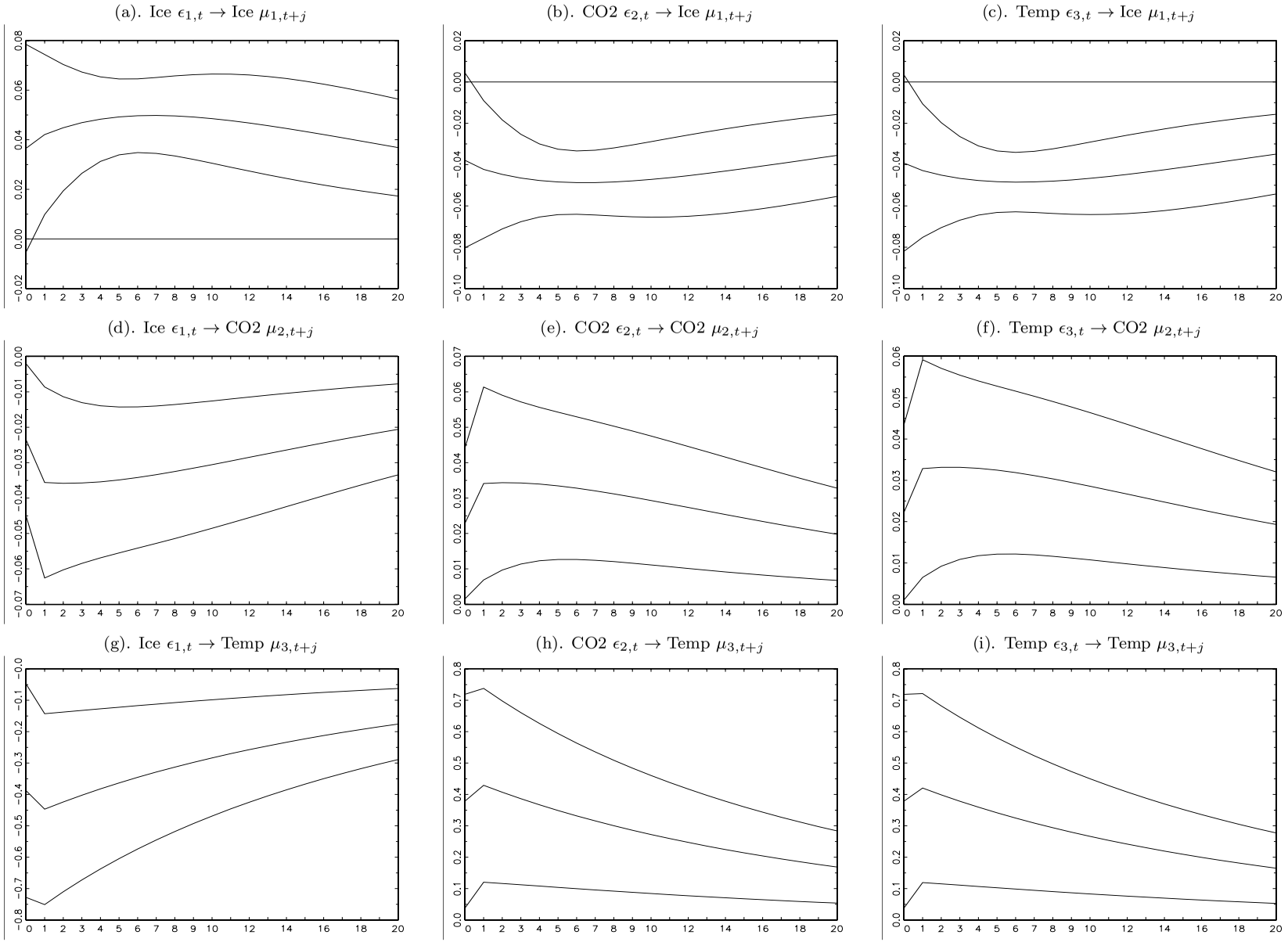

Figure 6. IRFs for the score-driven heteroskedastic ice-age model for the t-distribution.

Notes: The confidence interval is mean ± one standard deviation that is estimated for 1,698 out of the 3 million simulations, for which the restrictions of Table 1 are satisfied.

(a). $u_{1,t}$ as a function of $\epsilon_{1,t}$ and $\epsilon_{2,t}$

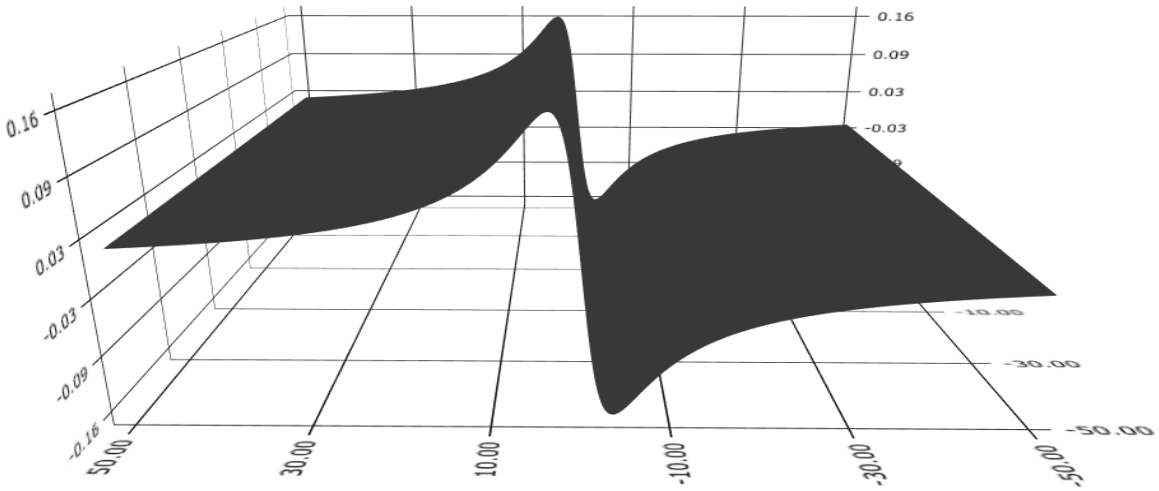

(b). $u_{2,t}$ as a function of $\epsilon_{1,t}$ and $\epsilon_{2,t}$

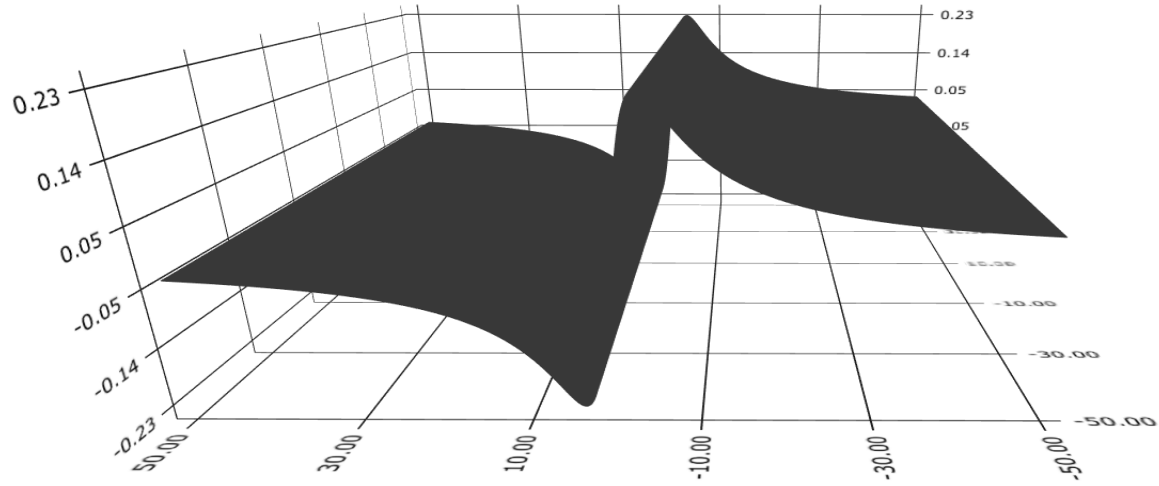

(c). $u_{3,t}$ as a function of $\epsilon_{1,t}$ and $\epsilon_{2,t}$

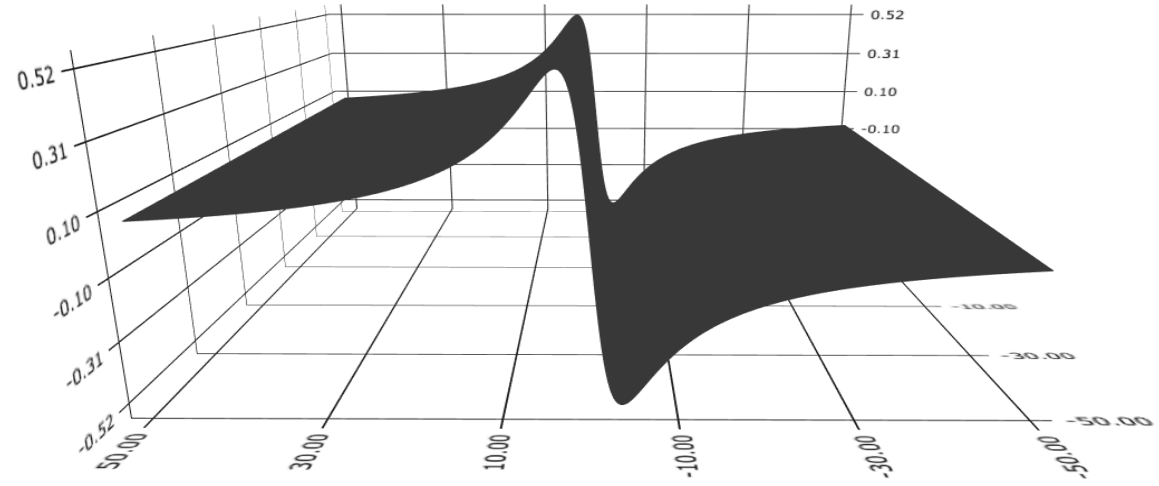

Figure 7. Robustness of the scaled score function to extreme values. *Note*: $\epsilon_{3,t} = 0$ is assumed for this figure.

3.2. Out-of-Sample Forecasting Results

In Table 5, the multi-step ahead out-of-sample forecasting performances of the (i) benchmark ice-age model (Castle and Hendry 2020), (ii) score-driven homoskedastic ice-age model for the normal distribution, (iii) score-driven homoskedastic ice-age model for the t-distribution, and (iv) score-driven heteroskedastic ice-age model for the t-distribution are compared.

The following climate variables are predicted: Ice_t, $\text{CO}_{2,t}$, and Temp_t. The estimation window is for the period of 798 thousand years ago to 101 thousand years ago ($T = 698$), for which humanity did not influence the Earth's climate. The multi-step ahead forecasting window is for the last 100 thousand years ($T_f = 100$). Due to the periods included in the estimation and forecasting windows, the forecasting results can disentangle the effects of humanity and the exogenous effects on the Earth's climate. We use two loss functions for forecasting performance evaluation: (i) mean square error (MSE), and (ii) mean absolute error (MAE). These loss functions are averaged for different periods of the last 100 thousand years (Table 5). We do not use statistical tests of forecasting accuracy, due to the small sample size.

For most of the cases, the MSE and MAE results indicate that, for the periods of the last 100 thousand years to the last 30-40 thousand years, the benchmark ice-age model provides the most precise forecasts (Table 5). The only exception for the MAE-based forecasting performance evaluation is for Ice_t, for which the results indicate that for the periods of the last 100 thousand years and the last 90 thousand years, the score-driven heteroskedastic ice-age model for the t-distribution provides the most precise forecasts (Table 5). The results also indicate for all variables that, for the most recent period of the last 20-30 thousand years, in which humanity impacted the Earth's climate, the score-driven homoskedastic ice-age model for the t-distribution provides the most precise forecasts (Table 5).

In Figure 8, the multi-step ahead out-of-sample forecasts of Ice_t, $\text{CO}_{2,t}$, and Temp_t for the (i) benchmark ice-age model, (ii) score-driven homoskedastic ice-age model for the normal distribution, (iii) score-driven homoskedastic ice-age model for the t-distribution, and (iv) score-driven heteroskedastic ice-age model for the t-distribution are presented.

The figure includes the observed values of Ice_t, $\text{CO}_{2,t}$, and Temp_t, the forecasts of these variables, and the forecasts $\pm$ one standard deviation estimates of the forecasts. The figure shows the following interesting results for the most recent period of the sample, when humanity impacted the Earth's climate (Castle and Hendry 2020). For the last 10-15 thousand years of the forecasting window, the observed values of ice are below the forecast interval, indicating unexpectedly low levels of ice. Moreover, for the last 10-15 thousand years of the forecasting window, the observed levels of CO_2 and temperature are above the forecast interval, indicating unexpectedly high levels of $\text{CO}_{2,t}$ and temperature. These multi-step ahead forecasting results are robust for the different econometric models (Figure 8), and are consistent with the results in the work of Castle and Hendry (2020, Figures 6.9, 6.12, and 6.13).

In Figure 9, the one-step ahead out-of-sample forecasts of Ice_t, $\text{CO}_{2,t}$, and Temp_t for the (i) benchmark ice-age model, (ii) score-driven homoskedastic ice-age model for the normal distribution, (iii) score-driven homoskedastic ice-age model for the t-distribution, and (iv) score-driven heteroskedastic ice-age model for the t-distribution are presented. We use a rolling-window approach for estimation and forecasting. The first rolling-window is for the period of 798 thousand years ago to 101 thousands years ago ($T = 698$). After the model estimation, the one-step ahead forecasts of all dependent variables are computed. Then, the first observation of the rolling-window is excluded and a new last observation is added from the sample. This estimation and the one-step ahead forecasting procedure is repeated until the end of the full sample period, providing $T_f = 100$ one-step ahead out-of-sample forecasts.

The figure includes the observed values of Ice_t, $\text{CO}_{2,t}$, and Temp_t, the forecasts of these variables, and the forecasts $\pm$ one standard deviation estimates of the forecasts. As for the multi-step ahead forecasts, for the last 10-15 thousand years, the figure shows a significant decrease in the level of ice and significant increases in CO_2 and temperature. For most of the periods of the last 10-15 thousand years, the observed values of ice are unexpectedly located below the mean forecasts, and the observed values of CO_2 and temperature are unexpectedly located above the mean forecasts. These forecasting results are robust for the different models.

Table 5. Multi-step ahead forecasts for the last 100,000 years.

	Benchmark ice-age model	Score-driven homoskedastic Gaussian ice-age model	Score-driven homoskedastic t ice-age model	Score-driven heteroskedastic t ice-age model	Benchmark ice-age model	Score-driven homoskedastic Gaussian ice-age model	Score-driven homoskedastic t ice-age model	Score-driven heteroskedastic t ice-age model
Ice_t	MSE	MSE	MSE	MSE	MAE	MAE	MAE	MAE
last 100000 years	**0.0917**	0.0982	0.0969	0.1005	0.2388	0.2520	0.2555	**0.2380**
last 90000 years	**0.1003**	0.1075	0.1058	0.1098	0.2535	0.2680	0.2713	**0.2515**
last 80000 years	**0.1081**	0.1169	0.1148	0.1205	**0.2661**	0.2830	0.2867	0.2664
last 70000 years	**0.1186**	0.1284	0.1258	0.1352	**0.2818**	0.3008	0.3044	0.2881
last 60000 years	**0.1259**	0.1370	0.1317	0.1526	**0.2848**	0.3063	0.3066	0.3097
last 50000 years	**0.1416**	0.1549	0.1472	0.1765	**0.3005**	0.3265	0.3238	0.3373
last 40000 years	**0.1712**	0.1868	0.1765	0.2150	**0.3444**	0.3738	0.3689	0.3914
last 30000 years	0.2148	0.2292	**0.2134**	0.2691	**0.3946**	0.4187	0.4080	0.4471
last 20000 years	0.3049	0.3164	**0.2911**	0.3767	0.5037	0.5143	**0.4948**	0.5575
last 10000 years	0.4889	0.5027	**0.4527**	0.6162	0.6935	0.7032	**0.6667**	0.7810
$\text{CO}_{2,t}$	MSE	MSE	MSE	MSE	MAE	MAE	MAE	MAE
last 100000 years	**0.0399**	0.0432	0.0424	0.0466	**0.1471**	0.1503	0.1506	0.1556
last 90000 years	**0.0440**	0.0479	0.0470	0.0517	**0.1580**	0.1642	0.1641	0.1709
last 80000 years	**0.0460**	0.0509	0.0494	0.0550	**0.1595**	0.1675	0.1664	0.1755
last 70000 years	**0.0513**	0.0568	0.0552	0.0623	**0.1719**	0.1810	0.1797	0.1920
last 60000 years	**0.0590**	0.0653	0.0634	0.0702	**0.1900**	0.1995	0.1986	0.2064
last 50000 years	**0.0692**	0.0769	0.0746	0.0831	**0.2128**	0.2254	0.2240	0.2352
last 40000 years	**0.0842**	0.0935	0.0902	0.1015	**0.2462**	0.2622	0.2598	0.2754
last 30000 years	**0.1104**	0.1214	0.1165	0.1313	**0.3089**	0.3263	0.3212	0.3404
last 20000 years	0.1269	0.1338	**0.1224**	0.1467	0.3261	0.3353	**0.3212**	0.3528
last 10000 years	0.1891	0.1978	**0.1733**	0.2221	0.4280	0.4379	**0.4088**	0.4664
Temp_t	MSE	MSE	MSE	MSE	MAE	MAE	MAE	MAE
last 100000 years	**4.1809**	4.5136	4.5168	4.8663	**1.6976**	1.7704	1.7906	1.8453
last 90000 years	**4.4536**	4.8600	4.8533	5.2546	**1.7714**	1.8574	1.8754	1.9406
last 80000 years	**4.5747**	5.1051	5.0628	5.4916	**1.7939**	1.9107	1.9207	1.9848
last 70000 years	**5.0599**	5.6824	5.6177	6.0398	**1.9174**	2.0581	2.0621	2.1106
last 60000 years	**5.7960**	6.5246	6.4482	6.8760	**2.1167**	2.2824	2.2886	2.3143
last 50000 years	**6.4533**	7.3840	7.2948	7.8500	**2.2670**	2.4787	2.4871	2.5283
last 40000 years	**7.3939**	8.3779	8.1927	9.0115	**2.4913**	2.7003	2.6894	2.7802
last 30000 years	**8.8750**	9.7268	9.3292	10.5446	**2.8029**	2.9516	2.8995	3.0520
last 20000 years	10.0692	10.5303	**9.5685**	11.9260	2.9566	3.0268	**2.8845**	3.2107
last 10000 years	14.0302	14.6377	**12.8303**	16.8965	3.7069	3.7892	**3.5384**	4.0858

Notes: Mean square error (MSE); mean absolute error (MAE). The lowest loss function values are indicated by bold numbers.

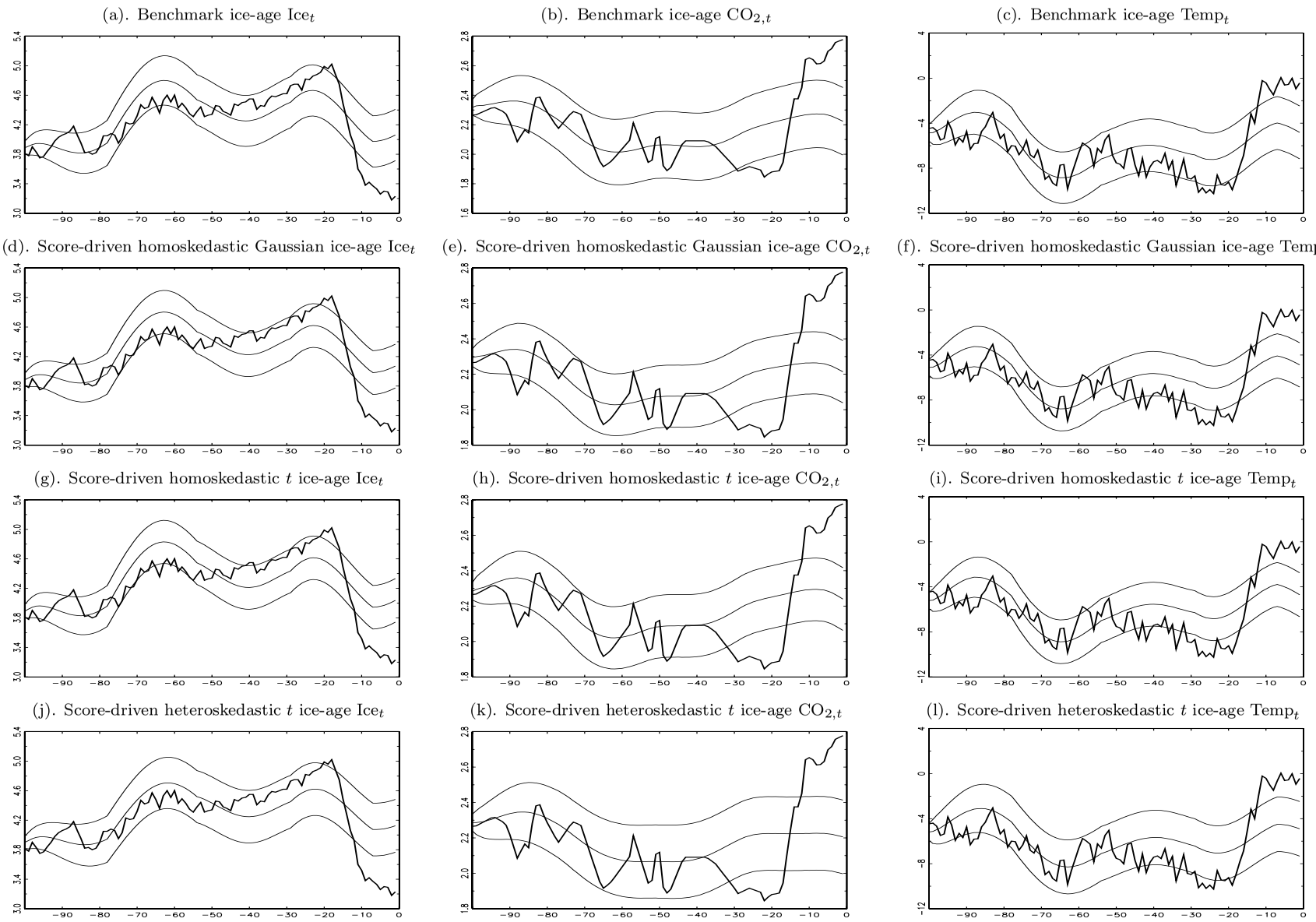

Figure 8. Multi-step ahead out-of-sample forecasts for the last 100 thousand years.
Notes: The confidence interval is mean ± one standard deviation. The true values are indicated by thick lines.

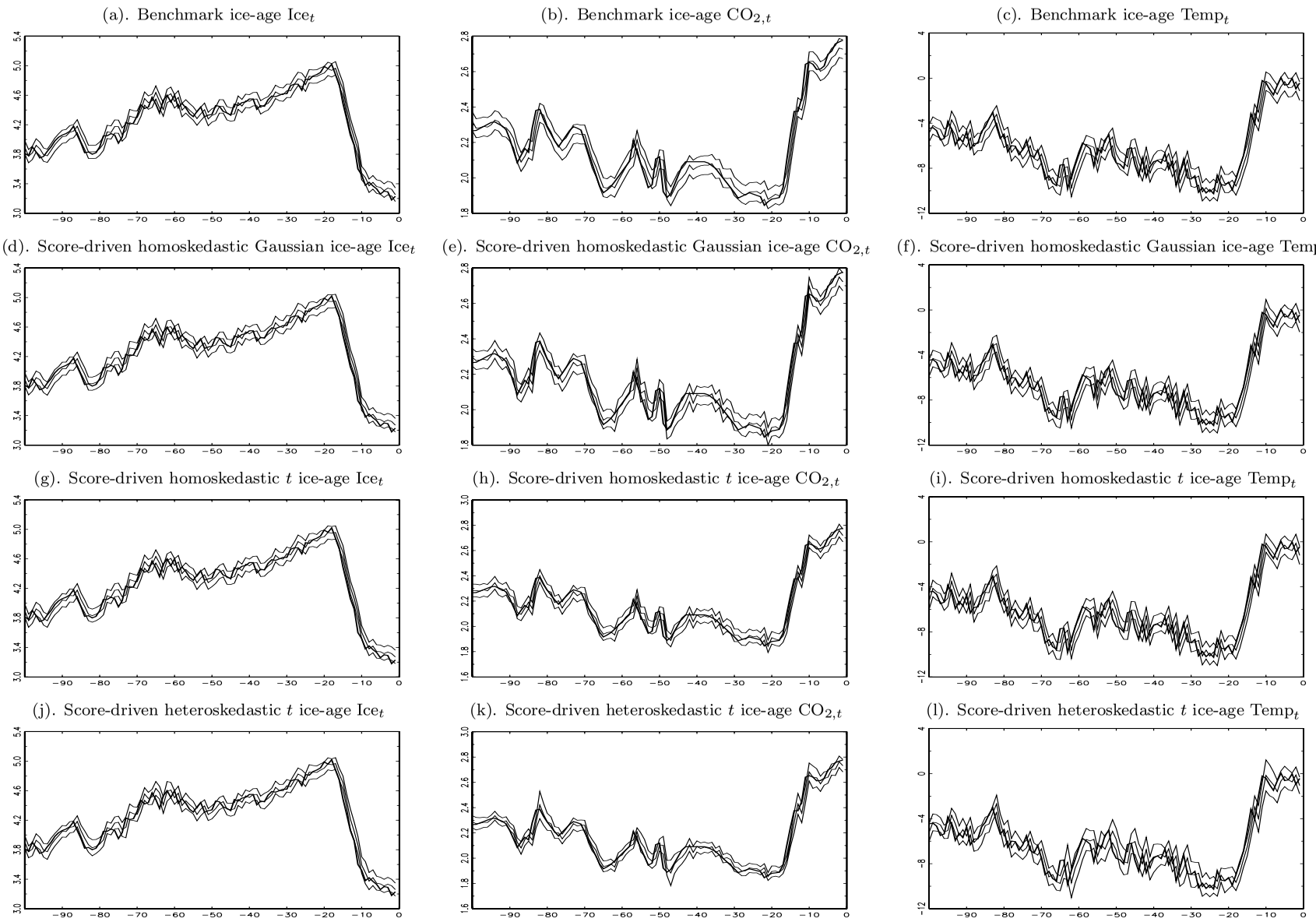

Figure 9. One-step ahead out-of-sample forecasts for the last 100 thousand years.
Notes: The confidence interval is mean ± one standard deviation. The true values are indicated by thick lines.

4. Discussion

We have compared the statistical and forecasting performances of the benchmark ice-age model (Castle and Hendry 2020) and those of our score-driven ice-age models. We have used data for climate and orbital variables for the last 798 thousand-year period, and we have provided out-of-sample forecasts of Antarctic ice volume, CO_2, and temperature for the last 100 thousand years. We have studied the robustness of the results of the benchmark model.

For data of the last 798 years, the statistical performance metrics and diagnostic tests have indicated that the dynamic specification of the benchmark ice-age model is improved. We have reported impulse responses among Antarctic ice volume, atmospheric CO2, and land surface temperature, which are robust for the specification of Castle and Hendry (2020). We have found that the average impact of a unit increase in the atmospheric CO2 level on land surface temperature is approximately 3.5 Celsius degrees for the benchmark ice-age model, and it is above 4 Celsius degrees for the score-driven models of our paper.

We have found that the forecasting results of the benchmark model are robust, by using data for the first 698 thousand years of the sample, for which humanity did not influence the Earth's climate, to forecast Antarctic ice volume, atmospheric CO_2, and land surface temperature for the last 100 thousand years of the sample. In this way, the effects of humanity and the effects of exogenous variables on the Earth's climate have been disentangled. For the last 10 to 15 thousand years when humanity influenced the Earth's climate, we have found the following results: (i) the forecasts of ice volume are above the observed ice volume, (ii) the forecasts of the atmospheric CO_2 level are below the observed CO_2 level, and (iii) the forecasts of temperature are below the observed temperature. These results help to disentangle the effects of humanity and the effects of the exogenous orbital variables on the Earth's climate, and they also a provide motivation to take further proactive actions to significantly reduce the greenhouse gas emissions, and to respond to the most important challenge of the 21th century: global warming.

Funding: Blazsek acknowledges funding from Universidad Francisco Marroquín. Escribano acknowledges funding from Ministerio de Economía, Industria y Competitividad (ECO2016-00105-001 and MDM 2014-0431), Comunidad de Madrid (MadEco-CM S2015/HUM-3444), and Agencia Estatal de Investigación (2019/00419/001).

Data Availability Statement: We greatly appreciate that Jennifer L. Castle and David F. Hendry provided us with the dataset of their work (i.e., Castle and Hendry 2020, Chapter 6). Data and computer codes are available from the authors of the present paper upon request.

Conflict of Interest: The authors declare no conflict of interest.

Acknowledgments: The authors are thankful for the comments of Matthew Copley and David Hendry.

References

Archer, David, Pamela Martin, Bruce Buffett, Victor Brovkin, Stefan Rahmstorf, and Andrey Ganopolski. 2004. The importance of ocean temperature to global biogeochemistry. *Earth and Planetary Science Letters* 222: 333–348. doi:10.1016/j.epsl.2004.03.011.

Blasques, Francisco, Janneke van Brummelen, Siem Jan Koopman, and Andre Lucas. 2021. Maximum likelihood estimation for score-driven models. *Journal of Econometrics*. doi:10.1016/j.jeconom.2021.06.003.

Blasques, Francisco, Siem Jan Koopman, and Andre Lucas. 2015. Information-theoretic optimality of observation-driven time series models for continuous responses. *Biometrika* 102 (2): 325–343. doi:10.1093/biomet/asu076.

Blazsek, Szabolcs, Alvaro Escribano, and Adrian Licht. 2020. Identification of seasonal effects in impulse responses using score-driven multivariate location models. *Journal of Econometric Methods* 10 (1): 53–66. doi:10.1515/jem-2020-0003.

Blazsek, Szabolcs, Alvaro Escribano, and Adrian Licht. 2021a. Co-integration with score-driven models: an application to US real GDP growth, US inflation rate, and effective federal funds rate. *Macroeconomic Dynamics*. doi:10.1017/S1365100521000365.

Blazsek, Szabolcs, Alvaro Escribano, and Adrian Licht. 2021b. Multivariate Markov-switching score-driven models: An application to the global crude oil market. *Studies in Nonlinear Dynamics & Econometrics*. doi:10.1515/snde-2020-0099.

Bollerslev, Tim 1986. Generalized autoregressive conditional heteroskedasticity. *Journal of Econometrics* 31 (3): 307–327. doi:10.1016/0304-4076(86)90063-1.

Box, George E. P., and Gwilym M. Jenkins. 1970. *Time Series Analysis, Forecasting and Control*. San Francisco: Holden-Day.

Bronselaer, Ben, Michael Winton, Stephen M. Griffies, William J. Hurlin, Keith B. Rodgers, Olga V. Sergienko, Roland J. Stouffer, and Joellen L. Russell. 2018. Change in future climate due to Antarctic meltwater. *Nature* 564: 53–58. doi:10.1038/s41586-018-0712-z.

Castle, Jennifer, and David F. Hendry. 2020. *Climate Econometrics: An Overview.* Foundations and Trends in Econometrics, vol. 10, no. 3–4, pp. 145–322. doi:10.1561/0800000037.

Creal, Drew, Siem Jan Koopman, and Andre Lucas. 2008. A general framework for observation driven time-varying parameter models. Tinbergen Institute Discussion Paper 08-108/4.
Available at: https://www.tinbergen.nl/discussion-paper/2649/08-108-4-a-general-framework-for-observation-driven-timevarying-parameter-models (accessed: 23 September 2021).

Creal, Drew, Siem Jan Koopman, and Andre Lucas. 2011. A dynamic multivariate heavy-tailed model for time-varying volatilities and correlations. *Journal of Business & Economic Statistics* 29 (4): 552–563. doi:10.1198/jbes.2011.10070.

Creal, Drew, Siem Jan Koopman, and Andre Lucas. 2013. Generalized autoregressive score models with applications. *Journal of Applied Econometrics* 28 (5): 777–795. doi:10.1002/jae.1279.

Doornik, Jurgen A. 2009. Autometrics. In *The Methodology and Practice of Econometrics.* Edited by Jennifer L. Castle and Neil Shephard. Oxford: Oxford University Press. 88–121.

Engle, Robert F. 1982. Autoregressive conditional heteroscedasticity with estimates of the variance of United Kingdom inflation. *Econometrica* 50 (4): 987–1007. doi:10.2307/1912773.

Engle, Robert 2002. Dynamic conditional correlation: A simple class of multivariate generalized autoregressive conditional heteroskedasticity models. Journal of Business & Economic Statistics 20 (3): 339–351. doi:10.1198/073500102288618487.

Harvey, Andrew C. 2013. *Dynamic Models for Volatility and Heavy Tails: With Applications to Financial and Economic Time Series*, Econometric Society Monographs. Cambridge: Cambridge University Press.

Harvey, Andrew C., and Tirthankar Chakravarty. 2008. Beta-t-(E)GARCH. Cambridge working papers in Economics 0840, Faculty of Economics, University of Cambridge, Cambridge. Available at: http://www.econ.cam.ac.uk/research/repec/cam/pdf/cwpe0840.pdf (accessed: 23 September 2021).

Intergovernmental Panel on Climate Change. 2021. Sixth assessment report. Available at: https://www.ipcc.ch/report/ar6/wg1/#SPM (accessed: 24 September 2021).

Jouzel, J., V. Masson-Delmotte, O. Cattani, G. Dreyfus, S. Falourd, and G. E. Hoffmann. 2007. Orbital and millennial Antarctic climate variability over the past 800,000 years. *Science* 317: 793–797. doi:10.1126/science.1141038.

Kibria, B. M. Golam, and Anwar H. Joarder. 2006. A short review of multivariate t-distribution. *Journal of Statistical Research* 40 (1): 59–72.

Lisiecki, Lorraine E., and Maureen E. Raymo. 2005. A pliocene-pleistocene stack of 57 globally distributed Benthic δ^{18}O records. *Paleoceanography* 20. doi:10.1029/2004PA001071.

Ljung, Greta M., and George E. P. Box. 1978. On a measure of lack of fit in time-series models. *Biometrika* 65 (2): 297–303. doi:10.1093/biomet/65.2.297.

Lüthi, Dieter, Marthine Le Floch, Bernhard Bereiter, Thomas Blunier, Jean-Marc Barnola, Urs Steigenhaler, Dominique Raynaud, Jean Jouzel, Hubertus Fischer, Kenji Kawamura, and Thomas F. Stocker. 2008. High-resolution carbon dioxide concentration record 650,000-800,000 years before present. *Nature* 453. doi:10.1038/nature06949.

Lütkepohl, Helmut 2005. *New Introduction to Multivariate Time Series Analysis*. Berlin Heidelberg: Springer-Verlag.

Paillard, Didier, Laurent D. Labeyrie, and Pascal Yiou. 1996. Macintosh program performs time-series analysis. *Eos Transactions AGU* 77 (39): 379–379. doi:10.1029/96EO00259.

Qin, Zhao, and Markus J. Buehler. 2012. Carbon dioxide enhances fragility of ice crystals. *Journal of Physics D: Applied Physics* 45 (44). doi:10.1088/0022-3727/45/44/445302.

Rubio-Ramirez, Juan F., Daniel Waggoner, and Tao Zha. 2010. Structural vector autoregressions: theory for identification and algorithms for inference. *Review of Economic Studies* 77 (2): 665–696. doi:10.1111/j.1467-937X.2009.00578.x.

Ruddiman, William 2005. *Plows, Plagues and Petroleum: How Humans Took Control of the Climate*. Princeton: Princeton University Press.

Wadham, J. L., J. R. Hawkings, L. Tarasov, L. J. Gregoire, R. G. M. Spencer, M. Gutjahr, A. Ridgwell, and K. E. Kohfeld. 2019. Ice sheets matter for the global carbon cycle. *Nature Communications* 10 (1). doi:10.1038/s41467-019-11394-4.

White, Halbert 2001. *Asymptotic Theory for Econometricians*, revised edition. San Diego: Academic Press.